

HOLISTIC SOLUTION METHODS FOR COMPLEX
MULTI-PARTICLE SYSTEMS

by

Wesley Krueger

A senior thesis submitted to the faculty of

Brigham Young University

in partial fulfillment of the requirements for the degree of

Bachelor of Science

Department of Physics and Astronomy

Brigham Young University

August 2010

Copyright © 2010 Wesley Krueger

All Rights Reserved

BRIGHAM YOUNG UNIVERSITY

DEPARTMENT APPROVAL

of a senior thesis submitted by

Wesley Krueger

This thesis has been reviewed by the research advisor, research coordinator,
and department chair and has been found to be satisfactory.

Date

Manuel Berrondo, Advisor

Date

Eric Hintz, Research Coordinator

Date

Ross L. Spencer, Chair

ABSTRACT

HOLISTIC SOLUTION METHODS FOR COMPLEX MULTI-PARTICLE SYSTEMS

Wesley Krueger

Department of Physics and Astronomy

Bachelor of Science

The emergence of self-organized behavior is characteristic of multi-particle systems in which individual motion is governed by the application of simple rules of interaction. The resulting dynamic order cannot be understood in terms of individual particles, but can be elucidated by formulating the system in terms of an abstract notion of dimensional coupling. We define this notion and consider two such systems in which the coupling rules are drawn from classical Newtonian mechanics. First we develop a deterministic flocking model based on the principles of consensus and frustration and demonstrate that both rules are required to elicit complex, flock-like behavior from the system. We then employ a quasi-stationary checkerboard lattice to develop a discretized damped Heisenberg model and demonstrate the spontaneous onset of magnetic domains. Finally, we discuss the importance of antagonistic interaction rules in the onset of complex, coherent dynamics away from equilibrium.

ACKNOWLEDGMENTS

To Dad, for not complaining (out loud) that I formatted his HP-41 to begin my explorations into the fascinating world of computer modeling. To Mom, for raising her eyebrows only slightly at every new scientific quest. To Mr. Raine and Mr. Francom, for encouraging the science obsession. To BYU, for putting up with me (and even giving me scholarships) for a long, long time. To Dr. Berrondo, for showing me the magic of vector calculus. To Dr. Berrondo, for patiently explaining why spin length is preserved—just one more time. To Almita, for allowing herself to be dragged to conference after conference to sleep through endless presentations in a doubly-foreign language.

Contents

Table of Contents	vii
List of Figures	ix
1 The Simple Rules of Complex Systems	1
2 Boids	7
3 The Heisenberg Model	25
4 Conclusion	59
Bibliography	65
A Phase Transitions in a Dynamic Flocking Model	69
B An Analytic Solution to the Gilbert Damping Equation	75
C Alternate Derivation of the Stereographic Projection	77
D Code for <i>pcolors3D</i>	81

List of Figures

2.1	Diagram of Non-Reciprocal Interaction Topology	15
2.2	States of Motion for Consensus-Only Boids Map	18
2.3	Time Evolution of the Consensus-Frustration Model	21
2.4	Sampling of Dynamic Structures in the Consensus-Frustration Model	22
3.1	Torque on a Spherical Pendulum	27
3.2	Spin Precessing about a Local Field	28
3.3	Spin Trajectories for Various Initial Energies	30
3.4	Spin Trajectory in the Stereographic Plane	37
3.5	Log Plot of Stereographic Trajectory Radius	37
3.6	Spin Trajectories for Various Initial Energies with Dissipation	39
3.7	Trajectories for Non-Interacting Spins	40
3.8	Small Two-Dimensional Spin Lattice	43
3.9	Quasi-Stationary Checkerboard Sublattices	43
3.10	Spin Lattice with Odd Number of Spins	45
3.11	Total Magnetization for Suzuki-Trotter Decomposition	48
3.12	Equilibria of Dissipative Spin Lattice	50
3.13	Lattice of 20 Spins with a Single Non-Zero Energy Spin	51
3.14	Energy Transfer between Two Coupled Spins	52
3.15	Energy Transfer Between Two Spins	53
3.16	3D Trajectory for a Single Spin	53
3.17	Color Map Representation of Spin Orientations	55
3.18	Onset and Evolution of Magnetic Domains	56
3.19	Magnetic Domains in Three Dimensions	58
A.1	Phase Transition from Aligned to Random Motion	71
A.2	Phase Transition from Rotational to Random Motion	72
A.3	Phase Transition between Linear and Rotational Motion	74
C.1	Geometric Inverse of a Scalar	77
C.2	Geometric Inverse of a Vector	78

Chapter 1

The Simple Rules of Complex Systems

Complexity is clearly ubiquitous throughout nature. From the fractal forms of clouds and coastlines, to the vast array of shapes, sizes, and colors in living organisms. From the intricate loops traced out by the driven damped pendulum to the unfathomable dances of whorls and eddies in a small stream. From the fascinating dynamics of flocks and schools containing thousands of individuals to the impenetrable interactions of the millions of neurons that make up the human brain. Complexity is the basis for the beauty of the natural world, but more enigmatically and certainly more importantly, complexity gives rise to structure and stability. Even more perplexing is the fact that the structures that arise from complex systems can seldom be understood by breaking the system into ever smaller constituent parts, and yet the emergent order is clearly recognizable and demonstrably subject to the basic laws of physics. Complex systems can also give rise to dynamic structure: schools of fish, evolutionary adaptation, and social networks. But what orchestrates this emergence of order? The answer lies in what we will refer to as dimensional coupling within the system.

A complex system is frequently defined as a system for which the whole is greater than the sum of its parts [10, 18]; that is, the behavior of the system as a whole cannot be elucidated by simply combining the low-level behaviors of the individual elements that make up the system. Nature is replete with examples: Quantum mechanical interactions tell us very little about the spontaneous formation and structure of clouds; the chemical and gravitational interactions between atoms and molecules do not offer completely satisfactory explanations for the formation of stars and galaxies; even combining our understanding of gas dynamics with the concept of forces is unable to shed much light on the details of a flag flapping in the breeze. Because the emergent behavior or properties of the system generally exhibit some overarching static or dynamic structure, we refer to the system as *self-organizing*. It is this self-organizing behavior that is not immediately apparent from the actions of individual parts—in fact, frequently the two two levels appear to be governed by completely independent and unrelated sets of rules or physical laws. In other words, turbulence does not follow from and cannot be better understood by the underlying quantum mechanical interactions that govern the fluid molecules; however, turbulence can be understood (to a degree) by fluid flow equations—in particular the Navier-Stokes equation. Likewise, the rise and fall of the stock market cannot be predicted based on the actions of individual shareholders (much to the dismay of Wall Street), but the boom and bust cycles have been demonstrated to follow power law distributions [3] and thus exhibit an overall order seemingly unrelated to individual purchases and sales. However, it is clear that emergent self-organization *does* depend in some way on the behavior of individual actors and frequently, once an emergent property has been understood according to some physical law, it can be shown that the global behavior is in fact consistent with the laws governing microscopic (compared to the global scale of the system) behavior. Solé and Goodwin state, “understanding the

molecular properties of H_2O does not allow us to derive the Navier-Stokes equations; having the Navier-Stokes equations does not give us a prediction and description of Bénard cells...We make [emergent self-organizing behavior] intelligible by recognizing how it is consistent with lower-level properties and by finding appropriate mathematical descriptors" [10]. Thus, complex systems do not lend themselves well to the reductionist techniques that have defined science for centuries; nevertheless, complexity does not spell the end of reductionism. The study of complex systems requires a holistic approach open to emergent phenomena and prepared to qualify and quantify self-organized behavior and reconcile this observed behavior with underlying physical laws, perhaps developing new insights into those laws as a result. Statistical mechanics and chaos theory provide some of the most common tools used in this holistic approach.

While strict reductionist techniques are not useful in attempting to understand complex systems, it is frequently helpful to divide such systems into several dimensions related to the degrees of freedom present within the system, thereby defining a type of phase space for the system. For example, a single gas molecule might have 6 independent dimensions related to its vector displacement and velocity; by extension, the phase space for a gas containing N molecules can be understood as a $6N$ dimensional system. In a similar manner, a multi-dimensional phase space can be defined for nearly any system, based on the physical properties of the system in question. This phase space turns out to be a very important tool in the analysis of complex systems, as it is the interaction, or coupling, between these dimensions that determines the emergent properties of the system.

While all complex systems can be viewed as multi-dimensional, not all multi-dimensional systems exhibit complex behavior. One obvious example is a low-density gas at equilibrium. As mentioned above, the phase space of such a gas will consist of

a vector position and velocity for each gas particle; however, these dimensions will, in general, remain essentially uncoupled across the gas—that is, in a dilute gas, particle-particle interactions are relatively infrequent and only occur during a brief moment of interaction. Thus the trajectory of each individual molecule evolves independently of the trajectories of the surrounding molecules, and any random interaction is eventually “undone” by another random interaction, due to the brevity and infrequent nature of the interactions. Since there is no dimensional coupling, there is no emergent behavior. This view is consistent with our physical understanding of a dilute gas at equilibrium: in such a gas, particle movement is essentially random—governed mostly by the temperature (and thus the kinetic energy) of the individual molecules. While molecule-molecule interactions do occur, they are, by and large, statistically irrelevant to the overall behavior of the gas.

As stated above, the key to complex behavior in a given system is the coupling between dimensions—self organization and emergent behavior can only arise where dimensional coupling is present. This coupling is most easily expressed in terms of rules defining how each dimension depends on the others. The rules themselves need not be complex—in fact, very simple rules often give rise to easily and elegantly described systems that exhibit highly complex emergent properties—but they must be non-linear. Returning to the dilute gas example, we find that even if the brief interactions between molecules are taken as a coupling between dimensions (perhaps we increase the density of the gas so that interactions become more frequent), these interactions will be governed by non-relativistic conservation of momentum, which is a linear relationship. This means that the particle-particle interactions do not serve to drive the system toward emergent behavior, but rather average out to a net zero effect on the global dynamics of the system. Thus the behavior of many molecules in a short time is essentially identical (from a statistical point of view) to the behavior

of one molecule over a proportionately longer time period—given enough time, a single gas molecule will visit every nook and cranny in a room; likewise, a gas containing 10^{23} particles will fill every nook and cranny of the room in $1/10^{23}$ of the time. In this case, the global behavior of the gas offers no more information than the dynamics of a single, non-interacting molecule, which is a result of the linearity inherent to the system.

Non-linear rules can frequently be expressed in simple English statements, but they provide the mathematical basis for developing a computer model of the system. Computer models are a crucial component of the study of complex systems, as even the simplest non-linear rules become completely intractable when applied over the tens or hundreds of dimensions in the phase space of the system; computer models, however, allow us to qualitatively observe the evolution of the system and thereby develop quantitative descriptions of its emergent dynamic properties. Furthermore, building a model of a complex system based on simple rules, even if those rules are obviously contrived or patently unrealistic, may give rise to qualitatively correct behavior when compared to a real system, thus allowing us to gain possible novel insights into the inner workings of the real system or confirm new observations of the system.

The use of coupling rules also provides a convenient way to represent interactions between the system and its environment. A closed complex system may exhibit self-organization, but frequently the emergent behavior is uniform and merely suggests the qualitative properties of the natural system in question, rather than offering compelling insights into the system. This is because, with no external influence, the system will eventually reach a uniform equilibrium state that may exhibit some sort of order, but is not generally understood as a “complex” system. The emergent order that characterizes complex systems, on the other hand, generally occurs away

from equilibrium, the result of an antagonistic “tug-of-war” between the coupling rules driving the system toward an equilibrium state and the external influences that, in general, oppose such a state, by imposing some sort of physical or energetic constraint. In a sense then, the external influences tend to prevent the system from reaching equilibrium by “stirring it up”, so to speak. Thus, by inserting rules whereby the system is allowed to interact with the environment as well as rules for internal coupling, we can ensure the non-equilibrium conditions that characterize the onset of emergent behavior.

In this paper, we will develop two models of very different physical systems based on simple rules drawn from classical Newtonian mechanics and show that these models exhibit the expected qualitative emergent behavior. In Chapter 2 we develop a flocking model that exhibits spontaneous grouping of initially randomly oriented “boids” based on two rules of interaction we have termed “consensus” and “frustration”. We show that consensus only will lead to two types of uniform motion, and that the addition of frustration gives rise to a spectacular range of highly complex motion that qualitatively resembles flocking. In Chapter 3 we develop a Heisenberg model based on spin-spin interactions described by the Gilbert relaxation equation and demonstrate the spontaneous onset of magnetic domains and other emergent properties in a damped ferromagnetic model away from equilibrium. Finally, in Chapter 4, we discuss the dimensional coupling present in each system and how this coupling contributes to the emergent properties described in the corresponding chapters. We also discuss antagonistic rules provided by interaction with the environment and explore their role in symmetry breaking and the onset of structure and coherence.

Chapter 2

Boids

A Flocking Model

Flocking, schooling, and swarming offer possibly some of the most fascinating examples of complexity in the natural world, and have been a source of inspiration since ancient times [13]. How the “lowly” creatures are able to twist and dodge much faster than the eye can follow, while simultaneously avoiding dangerous and even fatal collisions with flockmates sometimes only inches away is a feat that modern traffic controllers have yet to reproduce; and yet small birds, fishes, and even insects are able to carry out complex maneuvers in three dimensions with seemingly little thought at all. In fact, the concepts of “group think”, “crowd sourcing”, and “swarm intelligence” have sought to take advantage of the lowly creatures’ ability to form highly cohesive, swiftly-moving groups able to make complex decisions about predator evasion, food sources, and shelter that benefit both the individual members and the group as a whole—all without following the lead of any particular individual. Thus, the study of flocking and swarming may even be essential to human progress, as we learn to utilize the decision-making capacities of large collections of individuals for the ben-

efit of humankind [8]. Len Fisher states that “One of the most important emergent properties a group can have is swarm intelligence, which allows a group to tackle and solve problems in a way that its individual members cannot” [8]. Flocking and swarming could have application in many areas involving large interacting groups of people including traffic and crowd control, the spread of epidemics, marketing and economics, and social networking. Aside from clear practical implications, flocking and swarming is a fascinating problem in its own right and will provide many insights into the adaptability and evolution of large groups of independent individuals.

In this chapter we will approach the problem of flocking from a physical and mathematical standpoint, developing a model based on simple mathematical rules of movement and interaction. We will demonstrate that the model exhibits rich dynamic behavior that qualitatively resembles the flocking and swarming behavior observed in birds and insects. We will also discuss how the tools of statistical mechanics may be used to quantify some of the emergent properties of the virtual flock.

As suggested above, perhaps one of the most compelling and perplexing characteristics of flocks, schools, and swarms (which will be hereinafter grouped together generically as “flocks”, while the phenomena of flocking, schooling, and swarming will be collectively referred to as “flocking”), is the fact that most large flocks do not appear to be organized by the actions of a particular individual or leader. This has been demonstrated in multiple studies, which have also revealed that each individual acts as both a “leader” and a “follower” [6]. A similar result was demonstrated by Potts in his studies of flocks of Dunlin (*Calidris alpina*). He states: “Birds were considered initiators [of a given manoeuvre] when they began the manoeuvre before the rest of the flock” [19]. But how can a flock remain cohesive if each individual is free to follow the lead of any other individual and also free to “initiate” any given manoeuvre? And what determines who should follow whom? As with all complex systems, there are

certain rules of interaction governing the actions of each individual, and, as we will demonstrate with our own flocking model, it is precisely these rules that lead to the emergence of the coherent behaviors observed.

A basic flocking model consists of several individuals all moving with some speed v_0 in a given direction, which we can specify by an angle θ . Clearly there will be no emergent behavior if v_0 and θ either remain constant or are allowed to vary in random ways—the model will simply represent a gas of non-interacting particles that is easily understood through basic statistical analysis. The rules that give rise to the onset of ordered behavior are the rules of interaction between individuals. This concept was first applied to a flocking model by Reynolds, who described three rules of interaction for cohesive flocking [20]:

1. Collision Avoidance: avoid collisions with nearby flockmates.
2. Velocity Matching: attempt to match velocity with nearby flockmates.
3. Flock Centering: attempt to stay close to nearby flockmates.

Reynolds' model creates a self-organizing flock of “boids” (a contraction of the term “bird-oid”, coined by Reynolds to describe the “virtual birds” that made up his flocking model [20]) that exhibits high cohesion between individuals and, upon slight modification of rule 1—avoid collisions with nearby flockmates *and external objects*—exhibits a very interesting ability to encounter and successfully navigate around obstacles without permanent disruption of flock cohesion. One important note is that each of these rules acts on both v_0 and θ —that is, each boid may alter its speed and direction in order to fulfill the three rules of interaction—and thus, while quite realistic, this model may still be too complex for careful physical analysis.

The essence of this model was captured (independently) by Tamás Vicsek and his colleagues in a highly simplified model of self-driven particles. Vicsek's model is based

on a collection of particles governed by a single rule of interaction: “at each time step a given particle driven with a constant absolute velocity assumes the average direction of motion of the particles in its neighborhood of radius r with some perturbation added” [24]. The coherent motion in this model depends, in large measure, on the size of the perturbation or “noise level” and also on the size of the radius of interaction. Motion ranges from very small only slightly cohesive groupings for large perturbations and small values of r , to smaller, more tightly bound groups moving in random directions for larger values of r and less noise, to nearly uniform, linear motion for all particles in the simulation for large r and very small levels of noise [24]. The resulting motion is emergent, arising from an initial randomly distributed group of particles with random initial orientations, and the direction of coherent motion, especially in the uniform case, is selected by the group in a spontaneous fashion that is entirely dependent on the interactions between particles [24]. Because it is based on individuals with constant speed and applies only a single rule to modify the direction of each flock member, this model offers ample opportunities for mathematical interpretation and the authors provide insights into the statistical and physical properties of the model—in particular, they discuss the presence of phase transitions from ordered to disordered behavior in the flock and draw an analogy between their model and the models of ferromagnetism. Furthermore, a complete mathematical analysis of Vicsek’s model was performed by Toner and Tu [22].

Like Vicsek’s model, our flocking model is based on a two-dimensional array of initially randomly oriented self-driven boids, each moving at a constant speed within an infinite space, simulated by the use of periodic boundary conditions; however, rather than adopting a single rule of interaction, we employ two simple rules that we have termed “consensus” and “frustration”, which will be described in more detail below. Furthermore, we make the additional simplification of removing the “noise”

factor included in Vicsek’s model. This has the advantage of establishing a completely deterministic model, facilitating the description of the resulting emergent behavior, and given the complex behavior of the system, this is not a limitation: Chaotic fluctuations are bound to appear with no need to include a random feature explicitly. In our model, each boid is assumed to spontaneously acquire the energy necessary to maintain its constant absolute velocity for as long as required and independently of the interactions—that is, our model represents an open system of self-propelled boids. The equations of motion for each individual take the form of two sets of Hamilton-like coupled equations derived from Newton’s laws. These are the rules that describe the dimensional coupling for the system; the phase space consists of the direction and velocity of each boid, and the details regarding *how* each boid maintains its speed or alters its direction is irrelevant to the onset of large-scale order, as discussed in Chapter 1. Thus, the velocity vector of each boid is updated as a function of its relationship with the other members of the flock, and the corresponding position is subsequently modified based on this new velocity. Mathematically, this can be expressed as follows:

Let $\mathbf{v}_i(n)$ be the two-dimensional velocity vector for boid i at time step n . The velocity vector at time step $n + 1$ will then be

$$\mathbf{v}_i(n + 1) = v_0 \mathbf{F}_i(\hat{v}(n)), \quad (2.1)$$

where v_0 represents the fixed speed of each boid and \mathbf{F}_i is a specific averaging function that updates the orientation of the i th boid based on a set of velocity orientations $\{\hat{v}\}$ using the rules of consensus and frustration described below. It is the function \mathbf{F}_i then, that specifies the interaction between boids (that is, the dimensional coupling). Note that \mathbf{F}_i is constructed so as to preserve the magnitude of the original velocity vector v_0 of each boid. The two-dimensional positions of each individual are then

updated as:

$$\mathbf{r}_i(n+1) = \mathbf{r}_i(n) + \mathbf{v}_i(n+1)\Delta t \quad (2.2)$$

for a discrete time step Δt , which is generally set to 1 in the simulation runs.

By calculating the resulting positions in this way, we create a difference equation map. It is important to point out that the map itself is the model, and not merely a representation or approximation of an underlying set of differential equations. Using a map, rather than a differential equation, allows for the onset of complex motion, as demonstrated by May [17] in his paper on the logistic map. At least three differential equations would be required for the onset of complex dynamics, while only a single difference equation is needed to achieve a similar effect [9]. Thus the difference equation itself is the basis for this model, and is not simply an approximation of an underlying differential equation.

Consensus

In its general form given in Eq. 2.1, the interaction function \mathbf{F}_i could take practically any form. In fact, designing \mathbf{F}_i to align the direction of the i th boid with the average direction of the velocities of the set of neighbors within a radius r reproduces Vicsek's model described above. However, rather than specify a given radius of interaction for each boid, as was done by both Reynolds and Vicsek, we have adopted a non-reciprocal topological interaction in which each boid aligns its direction of motion with the average direction of motion of a fixed number of flockmates, regardless of distance. We feel that the topological interaction is critical to the onset of the emergent behavior observed in our model—a fact born out by recent field studies [4]—and also addresses a particular weakness in the nearest neighbor model with regard to the physical aspects of flocking; that is, the nearest neighbors interaction paradigm allows each

boid to interact only with other boids within a set radius—individuals outside this radius are effectively invisible to the boid in question. Reynolds acknowledges this particular shortcoming: “The flock model presented here is actually a better model of a school or herd than a flock. Fish in murky water (and land animals with their inability to see past their herdmates) have a limited, short-range perception of their environment” [20]. He further states, “Birds, especially those on the outside of a flock, have excellent long-range ‘visual perception’. Presumably this allows widely separated flocks to join together. If the flock centering urge was completely localized, when two flocks go a certain distance apart they would ignore each other” [20]. In addition, studies carried out by Wayne Potts have suggested that long-range interaction may be crucial in a flock’s ability to react nearly instantaneously to a perceived threat. He proposes a “chorus-line” hypothesis, wherein any individual may instigate a given manoeuvre and demonstrates that the resulting “manoeuvre wave” will then propagate through the flock three times faster on average than would be possible if the birds were simply reacting to the movement of their nearest neighbors alone [19]. Recent research by Ballerini *et al.* also indicates that strong cohesion is better obtained through a topological rather than a metric interaction paradigm and demonstrates that flocks of starlings (*Sturnus vulgaris*) do seem to interact based on topological distance rather than metric distance [4]. They state:

Why a topological, and not a metric, interaction? Animal collective behavior is staged in a troubled natural environment. Hence, the interaction mechanism shaped by evolution must keep cohesion in the face of strong perturbations, of which predation is the most relevant. We believe that topological interaction is the only mechanism granting such robust cohesion and, therefore, higher biological fitness. A metric interaction is inadequate to cope with this problem: Whenever the interindividual

distance became larger than the metric range, interaction would vanish, cohesion would be lost, and stragglers would “evaporate” from the aggregation. A topological interaction, in contrast, is very robust, because its strength is the same at different densities. By interacting within a fixed number of individuals the aggregation can be either dense or sparse, change shape, fluctuate and even split, yet maintain the same degree of cohesion [4].

There is then, much theoretical and experimental evidence in favor of a topological interaction paradigm.

In addition to a novel topology of influence, our interaction function is also characterized by a non-reciprocal interaction structure, in which the i th boid is randomly assigned a parametrized, fixed number of topological neighbors, but those neighbors do not necessarily follow boid i directly; rather, they align themselves with an identical number of other topological neighbors. That is, for a flock of boids $\{a\dots z\}$ with velocity vectors $\{v_a\dots v_z\}$, if boid i aligns its velocity vector with velocities $\{v_j, v_k, v_l, v_m, v_n\}$, then boid j may align itself with $\{v_k, v_l, v_m, v_n, v_o\}$ or any other randomly assigned set of velocities, *excluding* v_i . However, v_i may be included in one or more alignment arrays for boids not included in the alignment array for boid i (for example, boid f may align with the set of velocities $\{v_g, v_h, v_i, v_j, v_k\}$). Due to the randomized nature of the initial configuration, this is most easily achieved in practice by assigning each boid to align itself with the M subsequent velocity vectors, taken in order from the full array, as described above. This paradigm is best illustrated graphically. Fig. 2.1 illustrates the non-reciprocity of our interaction topology and compares it to a nearest neighbors model for the same configuration.

The rule of consensus, then, dictates that each boid align its velocity vector in the average direction of its topological neighbors before updating its position. This

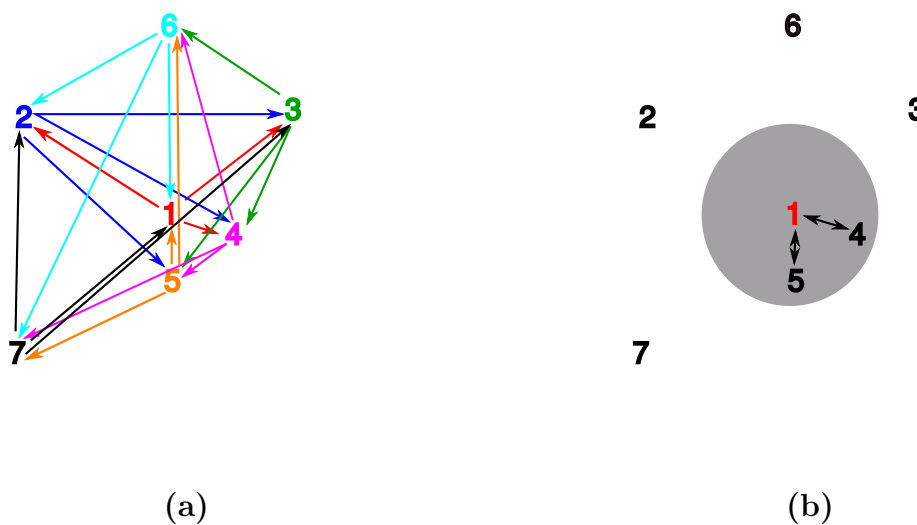


Figure 2.1 Diagram of the non-reciprocal interaction topology used in our flocking model. In this case, each member of a flock of N individuals follows M topological neighbors. (a) Diagram showing non-reciprocal interaction between a fixed number of flockmates. Note in particular that although boid n follows m , m does not directly follow n . (b) Diagram of a similar arrangement of boids showing nearest neighbor interaction for comparison.

average direction $\bar{\mathbf{v}}$ is calculated as follows:

$$\bar{\mathbf{v}} = \frac{\sum_{k=1}^M \mathbf{v}_k}{\left| \sum_{k=1}^M \mathbf{v}_k \right|}, \quad (2.3)$$

where each sum is taken over the M topological neighbors for the boid in question, assigned as described above and shown in Fig. 2.1. It is the normalization of $\bar{\mathbf{v}}$ in Eq. 2.3 that introduces the non-linearity that is so crucial to the emergent behavior of the model. The averaging function \mathbf{F}_i given in Eq. 2.1 is then simply:

$$\mathbf{F}_i(\hat{v}) = \bar{\mathbf{v}}_i, \quad (2.4)$$

where $\bar{\mathbf{v}}_i$ is the average direction of the topological neighbors for boid i , calculated using Eq. 2.3. Note that $|\mathbf{F}_i| = 1$, as required to conserve the absolute speed of each boid.

Starting from an array of randomly placed boids with random initial orientations and iterating Eqs. 2.1 and 2.2 over time, the model quickly reaches an equilibrium state of coherent motion. However, unlike the nearest neighbors models, which exhibit only uniform linear motion at equilibrium, the non-reciprocal topological interaction paradigm appears to introduce two additional forms of coherence: clockwise circular motion and counter-clockwise circular motion, in addition to the uniform linear motion observed in the nearest neighbors model. This circular motion is unique in the sense that the positions of each boid remain randomly scattered over the simulation space, but the motion of each individual becomes phase locked in a circular pattern, as shown in Fig. 2.2. These are dynamic phases of motion and very difficult to discern from snapshots of the simulation, as can be appreciated in Fig. 2.2. We have therefore included the paths of select numbers of boids to emphasize the motion taking place.

Despite the fact that the resulting motion is completely coherent and easily classified, these dynamics do exhibit the characteristics of complex phenomena. Although the overall motion of the “flock” is uniform, there are variations that arise from simulation to simulation, depending on the initial conditions. In the case of uniform linear motion, the final direction of motion is spontaneously determined by scaled long-range interactions among flockmates; likewise, the radii of the circles executed by the flock, while identical from boid to boid, will also vary based on the initial conditions and arise spontaneously from the interactions. Thus the states of motion are determined by the initial conditions and arise spontaneously from the scaling interactions into large-scale order. These states or phases of motion can be considered true “states” or “phases” in the thermodynamic sense, as we have found that by introducing a “noise” factor, similar to that used by Vicsek [24], the system exhibits first-order transitions from completely random motion to one of the ordered phases, and furthermore can also transition from linear to circular motion and *vice versa* as the noise factor is adjusted (analogous to the change in temperature that characterizes solid/liquid/gas phase transitions). A similar analysis in terms of phase transitions for our flocking model is given in Appendix A. The states of motion exhibited by our model are shown in Fig. 2.2, together with a completely random, non-interacting case ($M = 0$) for comparison.

Frustration

The uniform states of motion arising from the consensus-only model are of physical and mathematical interest, as they represent self-organizing behavior that is far richer than models based on nearest-neighbors interactions; however, while the model does demonstrate coherence, it does not exhibit the complex dynamics of true flocking

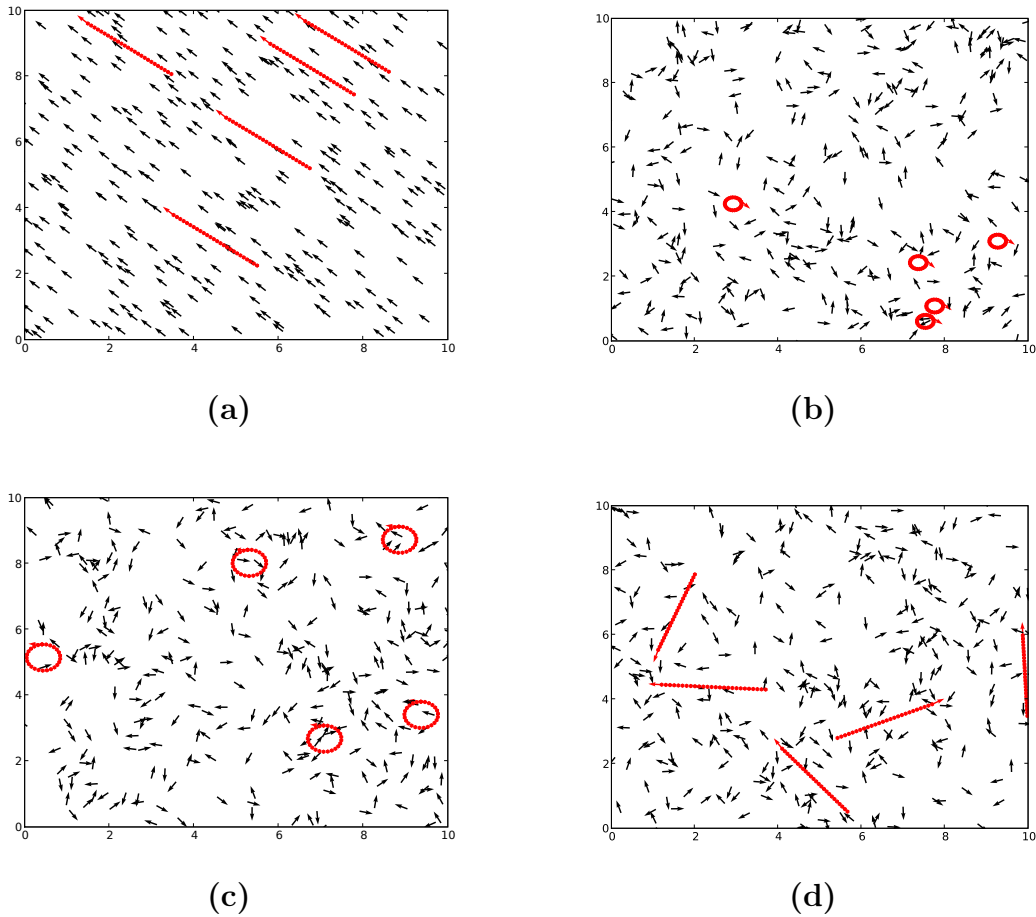


Figure 2.2 Motion obtained from a consensus-only map for $N = 300$ and $v_0 = 0.1$. The variations in the steady state behavior (direction of linear motion, radius of circular motion) are determined by the number of topological neighbors and the initial configuration of boids. Graph (a) shows the uniform linear motion obtained by our model and the nearest neighbors model. Graphs (b) and (c) show the clockwise and counter-clockwise circular motion unique to our model. Graph (d) shows the non-interacting case.

behavior—in short, it lacks *variability*, and thus lacks *adaptability*, both of which are required for flocking to be useful to the creatures that make up a flock, and are also characteristic of true complex systems [18].

Surprisingly, this variability can be obtained by the addition of a single, very simple rule, that we have termed frustration, as it places barriers on (frustrates) the flock’s tendency toward uniform motion. In fact, frustration is critical to the non-uniform, cohesive behavior observed in our model.

The simplest way to add frustration to the consensus model described above is to remove the periodic boundary conditions and place the boids in a circular, reflective boundary. Upon reaching the boundary, each boid is “reflected” by altering the direction of its velocity vector so as to prohibit crossing the boundary. Thus the frustration rule can be contained within the interaction function \mathbf{F}_i and overrides interaction with flockmates in the event the boundary is reached. Thus \mathbf{F}_i can now be expressed as:

$$\mathbf{F}_i(\hat{v}) = \begin{cases} \bar{\mathbf{v}}_i & \text{away from the boundary,} \\ \mathbf{f}(\mathbf{v}_{old}) & \text{at the boundary,} \end{cases} \quad (2.5)$$

where $\bar{\mathbf{v}}_i$ is calculated using Eq. 2.3 as before, \mathbf{v}_{old} is the velocity vector of boid i upon reaching the boundary, and $\mathbf{f}(\mathbf{v})$ is a function defined to act individually on each boid’s velocity vector as it reaches the boundary.

The boundary function \mathbf{f} has a highly significant effect on the dynamics of the flock. While there are countless ways to define how each boid should interact with the boundary, one simple yet very interesting interaction is to cause each boid to reflect by π at the boundary, thus

$$\mathbf{f}(\mathbf{v}) = -\mathbf{v}.$$

That is, each boid executes a “U-turn” upon encountering the boundary, returning back in the same direction it came. While this may seem somewhat unrealistic for birds, fish do seem to exhibit this type of behavior [5]. In any case, this particular boundary function appears to “maximize” the frustration in some sense.

The result of combining this frustration rule with the consensus rule described above is spectacularly unexpected and fully unexplainable in terms of the interactions that give rise to the emergent behavior. The combination of the boid-boid interactions and frustration at the boundary gives rise to a rich variety of coherent behavior that is non-uniform and yet surprisingly robust. Furthermore, the resulting dynamics exhibit the ability to vary in structure without destroying the coherence of the flock and *during a single run* may expand to occupy the entire perimeter of the simulation space only to later collapse into a very small cluster that moves as a single entity around the space. Possibly the most interesting characteristic of this “u-turn” boundary rule is the fact that it gives rise to very dense clustering, especially with large numbers of neighbors, and the resulting motion is very diverse: clustering at the boundary, rebounding as a tightly bound group, expanding and contracting, swirling, and seething as the flock traverses the simulation space and forming ever new and fascinating formations as the flock interacts among neighbors and at the boundary. Naturally, the initial conditions play an important role in the structures that ultimately form from these interactions, but the onset and evolution of such structures is determined almost entirely from the two simple rules of consensus and frustration.

It is clearly impossible to adequately represent the fascinating dynamics of the full flocking model in a static medium such as the printed page. However, in Fig. 2.3 we present a sequence of snapshots showing the evolution of one of the structures arising from our model. Then, in Fig. 2.4, we present a sampling of the wide variety of dynamic structures that form based on the modification of the parameters (number

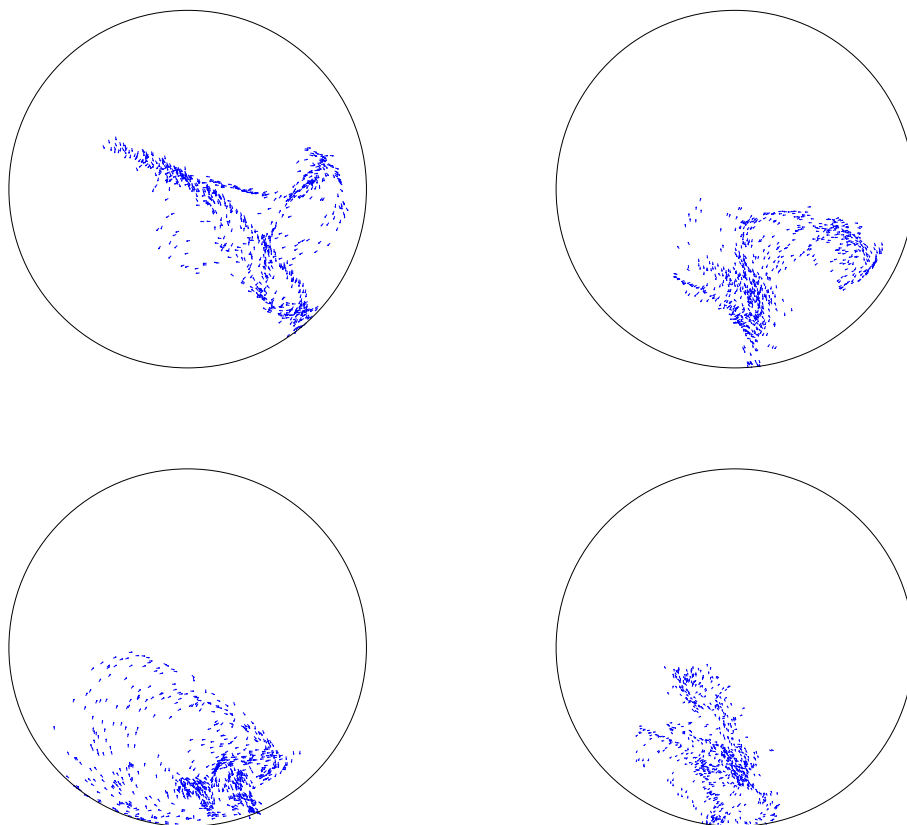


Figure 2.3 A sequence of 4 snapshots, 25 time steps apart, showing the time evolution of a single dynamic structure formed by the consensus-frustration model for a flock of 750 boids each following 13 topographical neighbors. The sequence begins with the upper leftmost image and progresses horizontally, left to right, ending with the bottom rightmost image.

of neighbors, density of boids).

As explained above, the behavior of the consensus-only model can be easily understood in terms of phase transitions. Physical analysis of the full consensus-frustration model is somewhat more difficult and is currently an ongoing project. Perhaps one of the most remarkable characteristics of the full consensus-frustration model is the tendency of the boids to become concentrated into a group much smaller than the total area of the simulation space, rather than becoming dispersed across it. However,

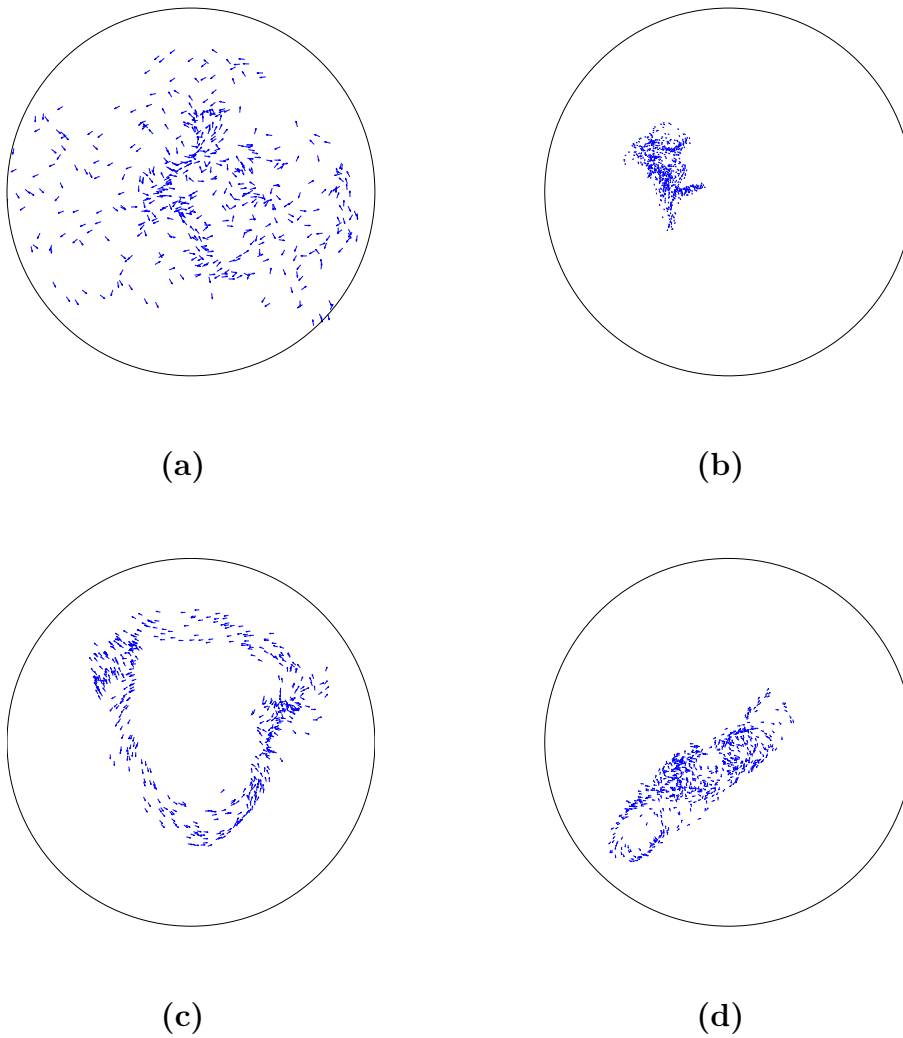


Figure 2.4 A sample of the dynamic structures produced by the consensus-frustration flocking model. (a) A flock of 500 boids, each following 4 topographical neighbors. (b) A flock of 800 boids, each with 25 topographical neighbors. (c) A flock of 500 boids, each with 10 topographical neighbors. (d) A flock of 650 boids, each with 10 topographical neighbors.

the enormous variety of behaviors exhibited by the model defies any simple thermodynamic explanation. Simulations comparing initial conditions differing only by the position of a single boid suggest that the tools of chaos theory may be useful in characterizing the motion observed in this model. The reflection by π at the boundary and the asymmetry in the boid-boid interactions that tend to induce rotational motion at both the individual and group levels suggest that an order parameter analogous to angular momentum may also be useful in understanding the overall behavior of the flock. In any event, the complex behavior exhibited by this model certainly warrants further study.

Chapter 3

The Heisenberg Model

The Heisenberg model is another system that exhibits complex dynamics and emergent properties. In essence, the Heisenberg model can be understood as a logical continuation of the boids model—that is, a flock of regularly spaced boids with initially random orientations and a very small velocity that align themselves according to the total alignment of a set of defined neighbors. The critical difference is in the interaction itself—rather than simply align each particle in the average direction of its neighbors, in the Heisenberg model we must account for the 3-dimensional precession of each spin about its local field, which is in turn determined by the orientation of its neighbors.

The Heisenberg model is the quintessential model of ferromagnetism or antiferromagnetism in materials. The model is based on the fact that a ferromagnetic (or antiferromagnetic) material can be understood as a conglomeration of tiny magnetic dipoles (spins) that are transversely fixed in a lattice structure, but free to rotate and orient themselves parallel or antiparallel to an influencing magnetic field. The individual magnetic fields of these spins then combine to create the macroscopic magnetic properties of the lattice as a whole.

In the presence of a very large external magnetic field, each spin will precess about a local axis pointing in the direction of the external field, with little influence from its neighbors. The solution in this case is straightforward and exhibits no complex or emergent properties and we will mention it only briefly. However, self-organization and other emergent phenomena do arise when each spin is allowed to interact with its nearest neighbors. The interaction arises because each spin sees a local field that is the sum of the dipole moments of its six nearest neighbors (in the case of a 3-dimensional lattice); however, this local field does not remain stationary, as the nearest neighbors are also precessing about their local fields, which are the result of their nearest neighbors and so forth. This is a complex interaction that could easily prove a source of complex dynamics, and we will indeed demonstrate the emergence of macroscopic order that is characteristic of complex systems. The Heisenberg model has proven to be a highly successful model for ferromagnetism and has also been used with good success as a model for spin glasses. We expect that the use of novel neighbor topologies and frustration paradigms to explore the onset of unique macroscopic phenomena could further extend the applicability of the model, as in the case of the Ising model.

Single Spin Dynamics

Because the basic unit for the Heisenberg model is the single spin, it is important to develop the dynamics of a single spin before attempting to describe spin-spin interactions across an entire 3-dimensional lattice.

Left to itself, a single spin will tend to align with its local magnetic field. However, given energy, the spin will tend to precess about an axis parallel to the local field at an angle that depends on the amount of energy contained in the spin. This precession

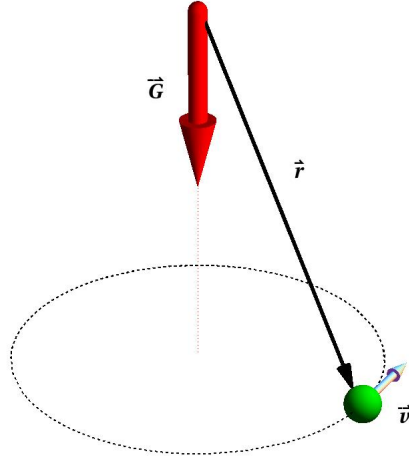


Figure 3.1 Torque on a spherical pendulum in a gravitational field.

is analogous to that undergone by a spherical pendulum in a gravitational field: with no energy, the pendulum will simply hang motionless downward; if given energy, the pendulum will precess about an axis parallel to the local gravitational field, as shown in Fig. 3.1. This precession is caused by torque according to the equation

$$\mathbf{k} = \mathbf{r} \times \mathbf{F},$$

where \mathbf{k} is the torque and \mathbf{F} is the force acting on \mathbf{r} [12]. Thus the precession of a single spin can be understood as a generalization of the torque on a spherical pendulum (see Fig. 3.2). We can now exploit the torque equation to write down a classical equation of motion for a single spin in the presence of a local magnetic field:

$$\frac{d\mathbf{S}}{dt} = -\mathbf{H} \times \mathbf{S}, \quad (3.1)$$

where \mathbf{S} represents the spin vector and \mathbf{H} represents the local field. As with the spherical pendulum, the energy of the system is closely related to the angular orientation of \mathbf{S} with respect to \mathbf{H} ; that is, higher energy simply means that \mathbf{S} will point

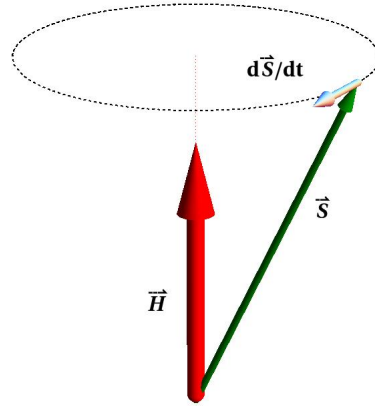


Figure 3.2 A spin \mathbf{S} precessing about a local field \mathbf{H} , as given by Eq. 3.1.

more antiparallel to \mathbf{H} . In this equation (and throughout this work), the energy of a spin system will be determined by the initial value of \mathbf{S} .

It is also important to note that Eq. 3.1 conserves spin length, which represents the magnitude of the dipole moment of the spin, as required for a physical ferromagnetic or antiferromagnetic system; thus, the spin may only take values lying on a sphere with radius $|\mathbf{S}|$, centered at the origin of \mathbf{S} .

Proof:

The length of the spin can be represented by

$$S^2 = \mathbf{S} \cdot \mathbf{S}.$$

Then by the product rule for differentiation

$$\frac{dS^2}{dt} = \mathbf{S} \cdot \frac{d\mathbf{S}}{dt} + \frac{d\mathbf{S}}{dt} \cdot \mathbf{S} = 2\mathbf{S} \cdot \frac{d\mathbf{S}}{dt},$$

since the dot product is commutative.

Now using Eq. 3.1

$$\frac{dS^2}{dt} = -2\mathbf{S} \cdot (\mathbf{H} \times \mathbf{S}) = 0,$$

and thus spin length remains constant in time, as required.

Eq. 3.1 is a linear equation in \mathbf{S} , and is easily solved analytically. Since we are working in a 3-dimensional space, the cross product can be written as the product of a skew-symmetric matrix and a vector in the following way:

Consider two vectors \mathbf{A} and \mathbf{B} , with components $[A_x \ A_y \ A_z]$ and $[B_x \ B_y \ B_z]$.

The cross product $\mathbf{A} \times \mathbf{B}$ is then

$$\mathbf{A} \times \mathbf{B} = \begin{vmatrix} \hat{i} & \hat{j} & \hat{k} \\ A_x & A_y & A_z \\ B_x & B_y & B_z \end{vmatrix} = \hat{i}(A_y B_z - A_z B_y) + \hat{j}(A_z B_x - A_x B_z) + \hat{k}(A_x B_y - A_y B_x).$$

Setting up an equivalent matrix multiplication gives

$$M(\mathbf{A}) \begin{pmatrix} B_x \\ B_y \\ B_z \end{pmatrix} = \begin{pmatrix} A_y B_z - A_z B_y \\ A_z B_x - A_x B_z \\ A_x B_y - A_y B_x \end{pmatrix},$$

where $M(\mathbf{A})$ is a matrix constructed using the components of \mathbf{A} such that, when multiplied by \mathbf{B} , it yields the equivalent of $\mathbf{A} \times \mathbf{B}$. It is then clear that the matrix operator $M(\mathbf{A})$ must then be:

$$\mathbf{A} \times \doteq \begin{pmatrix} 0 & -A_z & A_y \\ A_z & 0 & -A_x \\ -A_y & A_x & 0 \end{pmatrix}. \quad (3.2)$$

So, the equation of motion becomes:

$$\frac{d\mathbf{S}}{dt} = -\mathcal{H}\mathbf{S}, \quad (3.3)$$

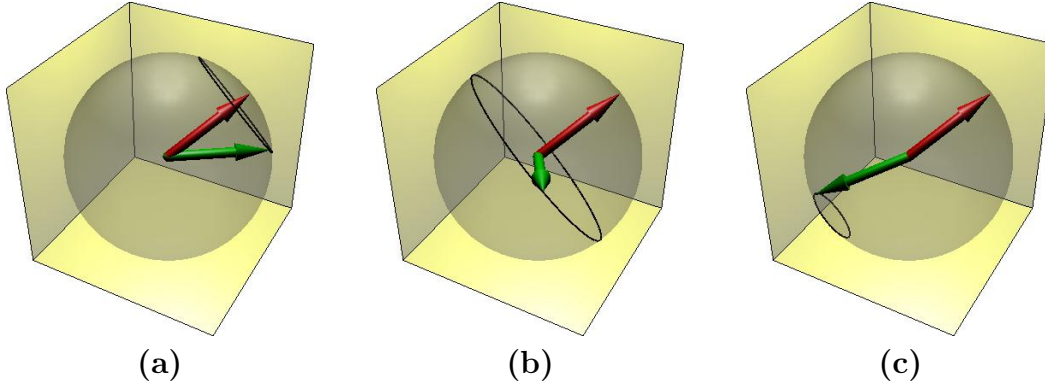


Figure 3.3 Trajectories for several spins with different initial energies. The local field \mathbf{H} is indicated by the red arrow, while the spin vector \mathbf{S} (at a given instant) is given by the green arrow. (a) Low energy case. (b) Medium energy case. (c) High energy case.

where \mathcal{H} is the skew symmetric matrix given by Eq. 3.2. Eq. 3.3 is a simple first-order vector differential equation, which can be easily solved in an analogous manner to the scalar equation $dx/dt = -\lambda x$. Thus the solution to Eq. 3.3 is:

$$\mathbf{S}(t) = e^{-(t-t_0)\mathcal{H}}\mathbf{S}(t_0), \quad (3.4)$$

where $e^{-(t-t_0)\mathcal{H}}$ represents the exponential of the matrix $-(t-t_0)\mathcal{H}$, which is well defined. Proof that this represents a rotation about the axis of \mathbf{H} is given by Tsai, *et al* [23].

For computational purposes, it is also convenient to develop an iterative solution to Eq. 3.3, as this will allow us to model the evolution of the spin in time steps of τ :

$$\mathbf{S}(t + \tau) = e^{-\tau\mathcal{H}}\mathbf{S}(t). \quad (3.5)$$

The trajectories of several spins with high, medium, and low initial energies are shown in Fig. 3.3.

While the dynamics of the completely conservative single spin system is of interest in its own right, there is little to be had in terms of complexity, as complexity in general requires a non-linear system, and the equation of motion for a single spin

is clearly linear. As in the boids case developed in Chapter 2, one obvious way of injecting non-linearity into the system is to consider several coupled particles, thereby introducing a non-linear dimensional coupling. However, before discussing methods for placing several dynamic spins in a lattice, it is convenient to analyze the addition of damping in the single spin case, because, as alluded to in Chapter 1 and demonstrated by concrete example in Chapter 2, the inclusion of an antagonistic element is also critical to the onset of large-scale order; and as we will demonstrate, allowing energy to dissipate out of the system entirely provides a sufficient “frustration” factor for the emergence of very interesting phenomena in the Heisenberg model.

Dissipation is typically added to a dynamical spin system upon the addition of the so-called Gilbert relaxation term, which modifies Eq. 3.1 as follows:

$$\frac{d\mathbf{S}}{dt} = -\mathbf{H} \times \mathbf{S} - \lambda \mathbf{S} \times (\mathbf{S} \times \mathbf{H}), \quad (3.6)$$

where λ represents the relative strength of the relaxation (the so-called “damping factor”). As in the conservative case, it is critical that the damping term preserve spin length. Proof that the Gilbert relaxation term does in fact fulfill this requirement is very similar to the proof that spin length is conserved for the non-dissipative case above. This time using Eq. 3.6, we have

$$\frac{dS^2}{dt} = 2\mathbf{S} \cdot [\mathbf{S} \times \mathbf{H} - \lambda \mathbf{S} \times (\mathbf{S} \times \mathbf{H})] = 2\mathbf{S} \cdot (\mathbf{S} \times \mathbf{H}) - 2\lambda \mathbf{S} \cdot [\mathbf{S} \times (\mathbf{S} \times \mathbf{H})].$$

The first term is zero as in the undamped case, and the second term must also be zero, since $\mathbf{S} \times (\mathbf{S} \times \mathbf{H})$ is perpendicular to \mathbf{S} . Thus

$$\frac{dS^2}{dt} = 0,$$

and spin length remains constant in time, as required.

Eq. 3.6 is a non-linear vector equation that can in fact be solved analytically if the local field \mathbf{H} is taken to be constant. While an analytic solution can be found in

Cartesian coordinates, as shown in Appendix B, the solution obtained is rather awkward to use if \mathbf{H} is allowed to change direction, as it requires several computationally intensive coordinate transformations. A much more elegant solution was proposed by Lakshmanan and Nakamura [15], who demonstrate that the stereographic projection onto the the plane perpendicular to the direction of the local field reduces the damping term $\lambda \mathbf{S} \times (\mathbf{S} \times \mathbf{H})$ to a simple constant rescaling of the time-step in the trajectory equation (Eq. 3.5). For the Heisenberg model involving many interacting spins we need a generalization of their result. Lakshmanan and Nakamura derive their solution by stereographic projection into the complex plane; however, appealing to the Möbius transformation, it is a simple matter to derive a basis independent vector solution, which has the additional advantage of eliminating the complex conjugate present in Lakshmanan and Nakamura's solution [15].

We start with the Möbius transformation

$$\omega = \frac{az + b}{cz + d}, \quad (3.7)$$

where z is the complex number to be transformed, ω is the transformation of z , and a , b , c , and d are complex constants. Taking $c \neq 0$, equation 3.7 can be rewritten as

$$\omega = A + \frac{1}{Bz + C}, \quad (3.8)$$

where A , B , and C are combinations of the constants a , b , c , and d above. Now B is a complex number of the form

$$B = |B| e^{i\phi}. \quad (3.9)$$

For our specific case we do not require the rotation given by the $e^{i\phi}$ factor, and we can take B as a real constant β , so

$$\omega = A + \frac{\beta}{z + C}. \quad (3.10)$$

Because there is a one-to-one correspondence between the complex planes represented by ω and z and a vector in 2-space, we can immediately write

$$\omega = \mathbf{a} + \frac{\beta}{\mathbf{r} + \mathbf{c}}, \quad (3.11)$$

where ω is a Möbius transformation of an arbitrary vector \mathbf{r} , \mathbf{a} and \mathbf{c} are constant vectors, and β is a constant scalar. However, because we have eliminated the possibility of a rotation (Eqs. 3.9 and 3.10), Eq. 3.11 is also true for vectors in any number of dimensions; in particular Eq. 3.11 now allows us to map three-dimensional vectors from one sphere onto another, based on the constants \mathbf{a} , \mathbf{c} , and β . To determine the appropriate values for \mathbf{a} , \mathbf{c} , and β , we can consider a unit sphere centered at an origin O and an infinite plane centered at a different origin O' . For a stereographic projection, the following conditions must hold:

1. if $\mathbf{r} = -\hat{\mathbf{n}}$ then $\omega = \infty$;
2. if $\mathbf{r} = \hat{\mathbf{n}}$ then $\omega = \mathbf{0}$;
3. if $\mathbf{r} = \mathbf{0}$ then $\omega = \hat{\mathbf{n}}'$;

where $\hat{\mathbf{n}}$ is a unit vector pointing from an origin O to the edge of the unit sphere centered at O , and $\hat{\mathbf{n}}'$ is a unit vector perpendicular to the plane centered at origin O' .

Applying these conditions to Eq. 3.11 and letting $\hat{\mathbf{n}}' = \hat{\mathbf{n}}$ (that is, letting the plane described by $\hat{\mathbf{n}}'$ be the tangent plane to the sphere at the point described by $\hat{\mathbf{n}}$) gives values for \mathbf{a} , \mathbf{c} , and β , yielding the final transformation

$$\omega = \frac{2}{\mathbf{r} + \hat{\mathbf{n}}} - \hat{\mathbf{n}} = \frac{2(\mathbf{r} + \hat{\mathbf{n}})}{(\mathbf{r} + \hat{\mathbf{n}})^2} - \hat{\mathbf{n}}, \quad (3.12)$$

where \mathbf{r} is an arbitrary vector, ω is the Möbius transformation of \mathbf{r} , and $\hat{\mathbf{n}}$ is the unit vector extending from the center of the unit sphere to the plane tangent to the sphere

(and therefore $\hat{\mathbf{n}}$ also describes the tangent plane). This is easily shown to meet the aforementioned conditions, and is thus the required transformation.

The reverse transformation is most easily obtained by using the inverse of a vector given in Appendix C and solving Eq. 3.12 for \mathbf{r} , thus

$$\mathbf{r} = \frac{2}{\omega + \hat{\mathbf{n}}} - \hat{\mathbf{n}}. \quad (3.13)$$

If we restrict our choices of \mathbf{r} such that all \mathbf{r} lie on the unit sphere tangent to the plane described by $\hat{\mathbf{n}}$, then Eq. 3.12 represents the stereographic projection of \mathbf{r} onto the plane described by $\hat{\mathbf{n}}$. This is done by letting $\mathbf{r} = \mathbf{S}$ and defining

$$S^2 = \mathbf{S} \cdot \mathbf{S} = 1, \quad (3.14)$$

$$S_n = \mathbf{S} \cdot \hat{\mathbf{n}}. \quad (3.15)$$

We can also define the components of \mathbf{S} parallel to and perpendicular to $\hat{\mathbf{n}}$

$$\mathbf{S}_{\parallel} = (\mathbf{S} \cdot \hat{\mathbf{n}})\hat{\mathbf{n}} = S_n \hat{\mathbf{n}}, \quad (3.16)$$

$$\mathbf{S}_{\perp} = \mathbf{S} - \mathbf{S}_{\parallel}. \quad (3.17)$$

Then

$$\boldsymbol{\Omega} = \frac{2(\mathbf{S} + \hat{\mathbf{n}})}{(\mathbf{S} + \hat{\mathbf{n}})^2} - \hat{\mathbf{n}}$$

and, applying the definitions 3.14, 3.15, and 3.17

$$\boldsymbol{\Omega} = \frac{\mathbf{S}_{\perp}}{S_n + 1}. \quad (3.18)$$

Thus $\boldsymbol{\Omega}$ (the stereographic projection of \mathbf{S}) has no component parallel to $\hat{\mathbf{n}}$ and must therefore lie on the plane described by $\hat{\mathbf{n}}$. As required by the conditions used in deriving the transformation Eq. 3.12, letting $\mathbf{S} = \hat{\mathbf{n}}$ gives $\boldsymbol{\Omega} = 0$ and letting $\mathbf{S} = -\hat{\mathbf{n}}$ gives $\boldsymbol{\Omega} = \infty$. Because all other points lying on the unit sphere will map uniquely to the tangent plane described by $\hat{\mathbf{n}}$, as given by Eq. 3.18, we have developed a

basis-independent method of calculating the stereographic projection of a spin \mathbf{S} in the plane described by the local field \mathbf{H} . Since the length of \mathbf{S} is conserved by the equations of motion, we can take $S^2 = 1$ with no loss in generality. Thus the stereographic projection of \mathbf{S} is given by

$$\mathbf{\Omega} = \frac{2(\mathbf{S} + \hat{\mathbf{n}})}{(\mathbf{S} + \hat{\mathbf{n}})^2} - \hat{\mathbf{n}} = \frac{\mathbf{S}_\perp}{1 + \mathbf{S} \cdot \hat{\mathbf{n}}}, \quad (3.19)$$

where \mathbf{S} is the spin vector, $\mathbf{\Omega}$ is the stereographic projection of \mathbf{S} , and $\hat{\mathbf{n}}$ is the unit vector in the direction of \mathbf{H} . For simulation purposes, it is useful to have the reverse transformation, from stereographic coordinates into Cartesian space. Taking Eq. 3.13 and again letting $\mathbf{r} = \mathbf{S}$ and $\omega = \mathbf{\Omega}$, we have (after some simplification)

$$\mathbf{S} = \frac{2(\mathbf{\Omega} + \hat{\mathbf{n}})}{1 + \mathbf{\Omega}^2} - \hat{\mathbf{n}}, \quad (3.20)$$

where we have used the planar condition $\mathbf{\Omega} \cdot \hat{\mathbf{n}} = 0$. We can now use the stereographic projection to solve Eq. 3.6. Starting with

$$\mathbf{S} = \mathbf{S}_\perp + \mathbf{S}_\parallel,$$

where \mathbf{S}_\perp and \mathbf{S}_\parallel are the components of \mathbf{S} perpendicular to and parallel to \mathbf{H} respectively, applying Eq. 3.19 and definition 3.16, and taking a time derivative gives (using dot notation for clarity):

$$\dot{\mathbf{S}} = \dot{S}_n \mathbf{\Omega} + (1 + S_n) \dot{\mathbf{\Omega}} + \dot{S}_n \hat{\mathbf{n}}. \quad (3.21)$$

From Eq. 3.6, we have

$$\dot{\mathbf{S}} = -\mathbf{H} \times \mathbf{S} + \lambda(\mathbf{H} - S_n \mathbf{H} \mathbf{S}). \quad (3.22)$$

Now taking the dot product of $\hat{\mathbf{n}}$ with Eq. 3.6, we obtain, after some simplification,

$$\dot{S}_n = \lambda H - \lambda H S_n^2 = \lambda H (1 - S_n^2). \quad (3.23)$$

Now substituting Eqs. 3.22 and 3.23 into Eq. 3.21, we have

$$-\mathbf{H} \times \mathbf{S} + \lambda(\mathbf{H} - S_n H \mathbf{S}) = \lambda H(1 - S_n^2)\mathbf{\Omega} + (1 + S_n)\dot{\mathbf{\Omega}} + \lambda H(1 - S_n^2)\hat{\mathbf{n}}.$$

After some simplification and deft application of definitions 3.16 and 3.17 and Eq. 3.19, we can eliminate all instances of \mathbf{S} and solve for $\dot{\mathbf{\Omega}}$, yielding

$$\dot{\mathbf{\Omega}} = -\mathbf{H} \times \mathbf{\Omega} - \lambda H \mathbf{\Omega}, \quad (3.24)$$

which is the stereographic differential equation of motion for spin precession with damping. Rewriting Eq. 3.24 as

$$\dot{\mathbf{\Omega}} = -(\lambda H + \mathcal{H})\mathbf{\Omega}, \quad (3.25)$$

where \mathcal{H} is the equivalent cross-product matrix defined in Eq. 3.3, we see that Eq. 3.6 has been reduced to a first order linear equation in the stereographic plane. Eq. 3.25 can be solved in an identical manner to Eq. 3.3, thus the trajectory of the spin vector in stereographic coordinates is a modified version of Eq. 3.5

$$\mathbf{\Omega}(t + \tau) = e^{-\lambda|\mathbf{H}|\tau} e^{-\tau\mathcal{H}} \mathbf{\Omega}(t), \quad (3.26)$$

where λ is the damping factor.

The stereographic projection offers a number of elegant geometric insights. First, the decay becomes exponential, which is typically observed in many damped or decaying systems, and by simply changing the sign of λ , we can model the dissipation ($\lambda < 0$) or injection ($\lambda > 0$) of energy, both of which give rise to an exponential change in the stereographic trajectory as shown in Figs. 3.4 and 3.5. Conversely, careful observation of the three-dimensional Cartesian trajectories illustrated in Fig. 3.6 show that this exponential decay is not at all obvious, and in fact does not even exist for the unit sphere. In addition, the two-dimensional stereographic view of the spin trajectory shows that dissipation of energy will bring the system to a zero point,

while injection of energy will send the system to infinity, which coincides with our physical understanding of many other dissipative systems. Finally, the stereographic projection constitutes a conformal mapping from Cartesian space to stereographic space, which means that each point on the unit sphere confining the spin trajectory will be mapped to a unique point in the stereographic plane and the angle between one spin position and the next will be preserved—thus the two-dimensional projection contains all the information found in the original three-dimensional problem, but is much easier to handle mathematically.

Using stereographic projection, the algorithm for calculating the trajectory for a single spin becomes the following:

1. Start with the local field \mathbf{H} for spin \mathbf{S} , and define $\hat{\mathbf{n}}$.
2. Use $\hat{\mathbf{n}}$ to calculate \mathbf{S}_{\parallel} and \mathbf{S}_{\perp} : $\mathbf{S}_{\parallel} = (\mathbf{S} \cdot \hat{\mathbf{n}})\hat{\mathbf{n}}$ and $\mathbf{S}_{\perp} = \mathbf{S} - \mathbf{S}_{\parallel}$.
3. Calculate Ω using Eq. 3.19.
4. Iterate Ω for the next time step using Eq. 3.26.
5. Calculate the new \mathbf{S}_{\perp} using Eq. 3.20.
6. Reconstruct \mathbf{S} : $\mathbf{S} = \mathbf{S}_{\perp} + \mathbf{S}_{\parallel} = \mathbf{S}_{\perp} + (\mathbf{S} \cdot \hat{\mathbf{n}})\hat{\mathbf{n}}$.

The trajectories of a single spin for various initial energies are shown in Fig. 3.6. Note that in each case, the spin tends to converge toward the direction of the local magnetic field.

Multiple Spin Dynamics

In theory, calculating the dynamics of several spins in a lattice is as simple as applying Eq. 3.5 or 3.26 to each spin, and indeed, if the dynamics in the presence of a very large

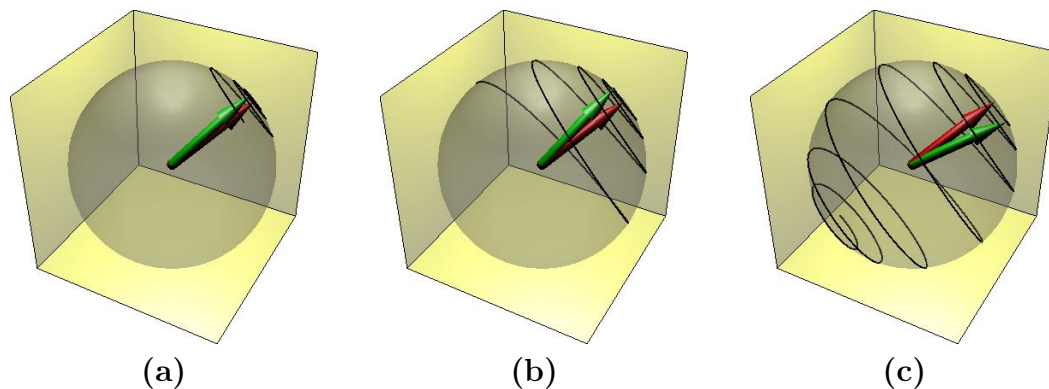


Figure 3.6 Trajectories for several spins with different initial energies. The local field \mathbf{H} about which the spin precesses is indicated by the red arrow, and the spin vector \mathbf{S} (at a given instant) is given by the green arrow. (a) Low energy case. (b) Medium energy case. (c) High energy case. The number of time steps in each case varies in order to demonstrate convergence toward \mathbf{H} .

external magnetic field—so large that spin-spin interactions become negligible—is desired, then individual application of the trajectory equations to each spin is sufficient. However, as can be appreciated in Fig. 3.7, this system offers no more information than a single isolated spin subject to the same equations: There will be no energy transfer between individual particles within the system, no transfer of energy into or out of the system, and certainly no complex behavior. Clearly, a different approach is required to model true physical systems and explore the complexity typically expected of such a multi-particle system. As with the boids model described in Chapter 2, the key to emergent behavior in this model lies in dimensional coupling, and the most natural way to introduce this coupling is through spin-spin interaction, so the phase space for a multiple-spin lattice will consist of the orientations of the individual spins.

The dynamics of the Heisenberg model is the result of precession of individual spins about their local magnetic fields. Up to this point, we have assumed a constant local field for each spin, but it is evident that by allowing this local field to change in time, we can alter the dynamics of a multiple spin lattice quite significantly. Furthermore,

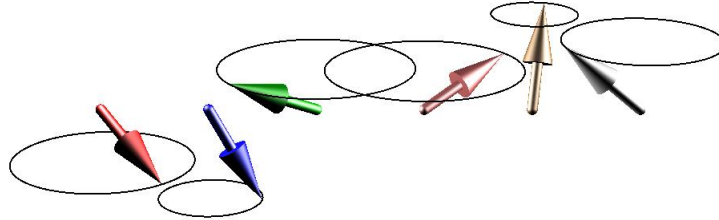


Figure 3.7 Trajectories for a 1D lattice of six non-interacting spins precessing about a constant magnetic field in the vertical direction. Each spin traces out a circle depending on its energy (compare to Fig. 3.3) and independent of its neighbors.

because each spin in the lattice is itself a magnetic dipole, each spin will create a small magnetic field that could affect nearby spins in some way. Therefore, by allowing the local field for each spin to include contributions from the magnetic fields of neighboring particles, we can introduce spin-spin interactions into the model without including additional interaction terms in the basic equations of motion used in the single spin case above (Eqs. 3.1 and 3.6). The most straightforward way to do this is to let the local field seen by each individual spin be the vector sum of the dipole moments of its nearest neighbors, where the nearest neighbors are defined in the typical way: In three dimensions in a cubic lattice structure, nearest neighbors include the particles directly above, below, to the left, to the right, in front and behind the particle in question, but not the particles at the diagonals. For the purposes of this thesis, we will be ignoring the presence of any external field, as we are focusing on internal particle coupling interactions, rather than the influence of external agents on the system—however, an external field could easily be included as an additional term in the sum of the nearest neighbor dipole moments. The local field for a particle i is

then given by

$$\mathbf{H}_i = \sum_j \mathbf{S}_j \quad (3.27)$$

over the j nearest neighbors of i . Furthermore, we will, for the most part, be using periodic boundary conditions; thus, for spins located at a boundary, nearest neighbors will include spins at the opposite boundary exactly vertical or horizontal (as the case may be) with respect to the spin in question.

At this point it is appropriate to introduce an interaction or coupling parameter J into Eqs. 3.1 and 3.6, which is simply a measure of the “strength” of the interaction between particles. For our purposes, the actual value of J is less relevant (it is most frequently used to model experimental results for specific materials [1,23]) than the *sign* of J , which will determine whether the system exhibits a tendency toward uniform alignment ($J > 0$) among all particles or uniform *anti*-alignment ($J < 0$). Thus the equations of motion become

$$\frac{d\mathbf{S}}{dt} = -J\mathbf{H} \times \mathbf{S} \quad (3.28)$$

in the undamped case, and

$$\frac{d\mathbf{S}}{dt} = -J\mathbf{H} \times \mathbf{S} - \lambda\mathbf{S} \times (\mathbf{S} \times \mathbf{H}) \quad (3.29)$$

for a damped system, where \mathbf{H} is defined by Eq. 3.27. Even at this level, unexpected complex behavior is suggested by the introduction of coupling between particles, as for a single particle, the changing the sign of the coupling parameter merely serves to reverse the direction of precession—it emphatically does not cause the spin in question to anti-align with its local field. This is clear upon inspection of Eqs. 3.5 and 3.26—insertion of a constant parameter J into the exponent will simply cause reversal of the direction of precession. Thus, Eqs. 3.6 and 3.29 will always cause the spin to align with its local field, and only multi-particle systems based on this model will

exhibit anti-alignment, because it is the interaction itself that ultimately determines the direction of the individual local fields \mathbf{H}_i .

Unfortunately, the exact solutions found in the previous section for a single spin are no longer directly valid in the case of multiple spins, as those solutions assume a *constant* local field \mathbf{H} , and in Eqs. 3.28 and 3.29, \mathbf{H} is a function of time, both in magnitude and direction, because it depends on the orientation of neighboring spins (Eq. 3.27), which clearly change with time. Furthermore, in a response [16] to the letter by Lakshmanan and Nakamura [15], it was demonstrated by Magyari, Thomas, and Weber that for a variable local field (generally arising from multiple spins), the stereographic projection that allows the damping factor to be handled as a rescaling of time is invalid. They state: “...the validity of the rescaling procedure proposed by Lakshmanan and Nakamura is strictly limited to the trivial case of a single spin in a constant magnetic field” [16]. However, by combining our basis-independent vector implementation of the stereographic projection with an integration method proposed by Tsai, Lee and Landau [23], we have developed an integrator that models the true dynamics of a damped Heisenberg lattice consisting of an arbitrary number of spins, and offers interesting insights into the complex behavior of ferromagnetic materials.

The key to performing accurate numerical integration in both the damped and non-damped cases is the division of the full spin lattice into two or more “quasi-stationary” sublattices. The concept is most easily illustrated through diagrams of a small, two-dimensional lattice.

Fig. 3.8 shows a small 2-D lattice of spins, represented by arrows. In this case, the nearest neighbors for each spin consist of the spins to the left, to the right, above, and below the spin in question. Periodic boundary conditions apply, so the corresponding topmost and bottommost spins will be coupled, as will the leftmost and rightmost spins. This can be illustrated graphically by dividing the lattice into

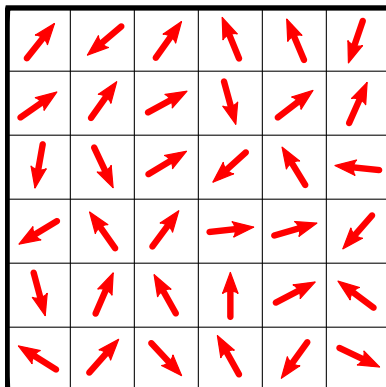


Figure 3.8 A small, two-dimensional lattice of randomly-oriented spins.

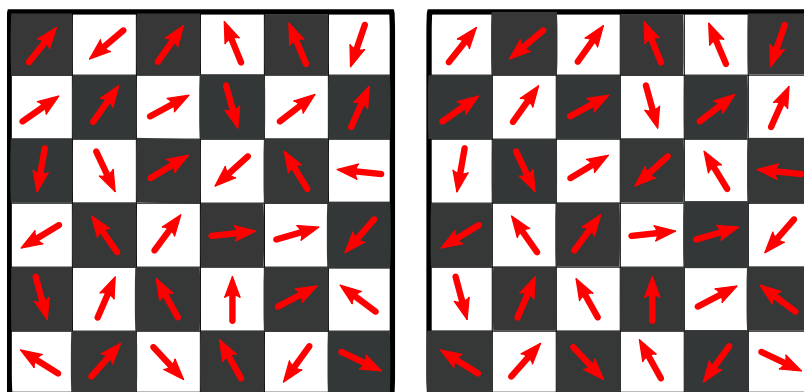


Figure 3.9 Quasi-stationary sublattices for nearest neighbor interaction with periodic boundary conditions.

two “checkerboard” sublattices, as shown in Fig. 3.9; thus the local field for each spin in a white square will be determined by the four adjacent black squares (jumping to the opposite side if at the boundary) and *vice versa*. This idea is easily generalized to three dimensions by adding spins perpendicular to the plane and taking the nearest neighbors in that direction also. This division into sublattices allows us hold one sublattice stationary while applying the precession equations to the other. For the instant in time that this small motion is considered to take place, the equations are valid because the local field (given by the “stationary” neighbors sublattice) remains essentially constant for the time step in question. We then switch sublattices and

process the second, while holding the first stationary. Thus, each sublattice can be considered “quasi-stationary”, while the other is allowed to evolve. The details of this method will be explained in greater detail in the following paragraphs. The distinct advantage of this method, is that it will conceivably allow for other topographical coupling schemes with little to no modification of general dynamics algorithm. The only requirement is that the coupling allow the lattice to be divided into two (or more) sublattices such that each spin is directly coupled only to spins in the opposite sublattice so that one sublattice can be held stationary while the other is allowed to evolve. This is critical to the successful implementation of this particular integration algorithm.

In the nearest neighbors case, this method fails drastically if the lattice contains an odd number (larger than one) of spins along any dimension and periodic boundary conditions are used, because, as illustrated in Fig. 3.10, it is impossible to create two independent, nearest neighbors sublattices as described above. At the boundary, there will always be some overlap between the two sublattices, due to the geometry of the lattice itself. In practice however, this is not as great a limitation as it may seem. Since the purpose of periodic boundary conditions is to emulate an infinite lattice, or at least a small volume near the center of an infinite lattice, the use of even or odd values in any given dimension will have no bearing on the final dynamics. As in thermodynamic analyses of large systems, the specific states of a complex system matter less than the overall dynamic behavior. While disregarding odd-valued lattices will cause us to miss the states specific to those configurations, the overall dynamic behavior will still be similar to that of the even-valued lattices. Thus the information we are interested in will still be present in our subset of possible configurations and we lose nothing by excluding odd-valued lattices.

By dividing the spin lattice into independent sublattices, we can ensure that for

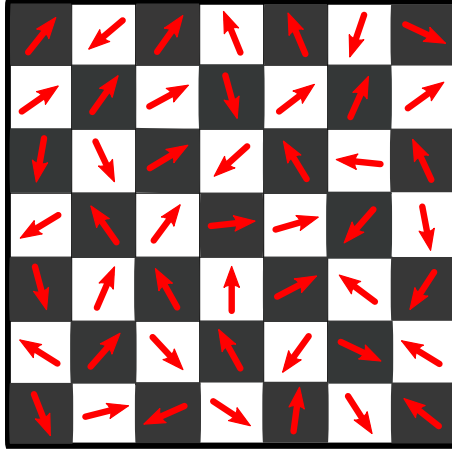


Figure 3.10 A two-dimensional spin lattice with 7 spins on a side. In this case division into two checkerboard sublattices (black and white) with periodic boundary conditions requires that, at the boundaries, spins in the black lattice orient themselves with other spins in the black sublattice (and likewise with the white sublattice), violating the quasi-stationary character of the two sublattices required by the integration algorithm.

a single time step, the local field seen by one sublattice as a result of the others will remain constant for that time step, and this will be true for every sublattice that makes up the full spin lattice. In particular, if we divide a spin lattice into two independent sublattices, A and B , we can define two local field matrices, \mathbb{H}_A and \mathbb{H}_B , which contain the local field cross product matrices, as defined for Eq. 3.3 and its solution, Eq. 3.5, corresponding to each spin in the appropriate lattice. Eq. 3.5 can now be written as

$$\mathbb{S}(t + \tau) = e^{-\tau(\mathbb{H}_A + \mathbb{H}_B)}\mathbb{S}(t), \quad (3.30)$$

where \mathbb{S} represents a matrix containing the vectors \mathbf{S} for each spin in the lattice and \mathbb{H}_A and \mathbb{H}_B are defined as above and do not commute. The exponential operator can however be factorized approximately for implementation in a decomposition algorithm [23]. The second order decomposition is equivalent to the Suzuki-Trotter

decomposition and gives the following result [23]:

$$e^{-\tau(\mathbb{H}_A+\mathbb{H}_B)} = e^{-\tau/2\mathbb{H}_B}e^{-\tau\mathbb{H}_A}e^{-\tau/2\mathbb{H}_B} + \mathcal{O}(\tau^3) \quad (3.31)$$

This symplectic implementation has the virtue of preserving the magnitude of each spin, as required by our model. It is equivalent to using a unitary approximation in solving quantum equations.

Thus the spins in sublattice A precess about their corresponding fields in \mathbb{H}_B , while the spins in sublattice B precess about the fields in matrix \mathbb{H}_A , and “because these operators rotate a spin around its effective field, which is fixed during this rotation, the scalar products of spins are preserved in each of these operations; therefore the spin length and the energy are conserved exactly (within machine precision).” [23] It is clear then, that this method relies on \mathbb{H}_A and \mathbb{H}_B remaining constant for the appropriate time step. If the sublattices were not completely independent, i.e. if even a single spin were influenced by members of the same sublattice or from both sublattices, the constant field assumption would break down, we could not ensure that spin length is conserved, and the integration would fail after only a few iterations.

The dynamics of a lattice of coupled spins can be calculated as follows: Starting from a lattice (one, two, or three-dimensional) of randomly oriented spins, divide the lattice into two “checkerboard” sublattices, based on nearest-neighbor interactions as described above. We will call these sublattices A and B for clarity. For each spin a_i in sublattice A , calculate the corresponding local field from the nearest neighbors in sublattice B and update the orientation of a_i according to Eqs. 3.5 and 3.31; that is,

$$\mathbf{a}_i(t + \tau) = e^{-\tau/2\mathcal{H}_i}\mathbf{a}_i(t), \quad (3.32)$$

where \mathcal{H}_i is the local field cross-product matrix as described in Eq. 3.2. Note the $\tau/2$ factor from the decomposition, which amounts essentially to half the required rotation of the spins in sublattice A . After performing this calculation for each spin

in sublattice A , we perform a similar calculation on each spin in sublattice B using the local fields created by the now modified sublattice A . Thus for each spin b_i in sublattice B , we calculate the corresponding local field and update its orientation by

$$\mathbf{b}_i(t + \tau) = e^{-\tau \mathcal{H}_i} \mathbf{b}_i(t), \quad (3.33)$$

which combines Eqs. 3.5 and 3.31 for sublattice B . Note that the rotation is performed for the full time step τ . Finally, we perform the second half of the rotation for sublattice A , using Eq. 3.32 as before, but now using the updated sublattice B to calculate the local fields for the spins in A . This cycle is repeated for as long as required to observe the dynamics of the system. The enormous advantage of this particular method is the fact that the time step τ may be made fairly large without adversely affecting the resulting dynamics [23].

In the non-dissipative case, we would expect that energy be conserved for the system, and therefore that the total magnetization remain constant throughout time. Tsai, *et al.* [23] perform a comprehensive analysis demonstrating that the decomposition algorithms do conserve both spin length and energy to machine precision, and also show that, on the order of the time steps in the simulation, total magnetization is not conserved exactly; that is, the algorithm does exhibit both positive and negative fluctuations in total magnetization at each time step. However, they also demonstrate that neither the second or fourth-order decomposition algorithms exhibit long-term drifts in magnetization. This is born out by our own implementation of the Suzuki-Trotter decomposition for a non-dissipative spin lattice. Fig. 3.11 shows the total magnetization over time for a three-dimensional $10 \times 10 \times 10$ lattice over 2000 time steps.

Treating a multiple-spin lattice with dissipation essentially combines the stereographic projection algorithm given for a single spin with the Suzuki-Trotter decom-

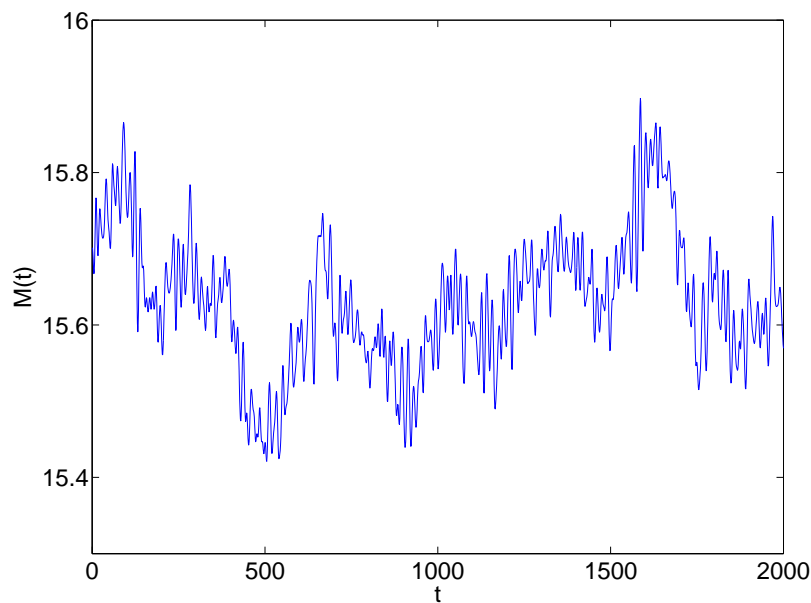


Figure 3.11 Total magnetization of a $10 \times 10 \times 10$ lattice of initially randomly oriented spins over 2000 time steps ($\tau = \pi/25$). The short-scale fluctuations both above and below the initial value are characteristic of the second-order Suzuki-Trotter decomposition algorithm. Note, however, that there is no clear upward or downward trend in total magnetization, indicating that the algorithm is effective for long-term dynamics.

position algorithm described above. In fine, the initial spin lattice is divided into two sublattices, as before. However, in this case, before applying Eqs. 3.32 and 3.33, each spin must be transformed to stereographic coordinates (see page 38 and Appendix B). After application of the pertinent equation (3.32 or 3.33 appropriately transformed to stereographic coordinates as in Eq. 3.26), the spin must then be transformed back to the unit sphere in 3-d Cartesian coordinates before proceeding to the next lattice.

Because it is an open system, the dissipative spin lattice clearly does not conserve energy and therefore cannot be expected to conserve its initial magnetization, which it does not. However, it does manifest the expected tendency toward full alignment or anti-alignment of all members of the lattice, depending on the sign of the coupling parameter J (see page 41 and Eq. 3.29), as shown in Fig. 3.12.

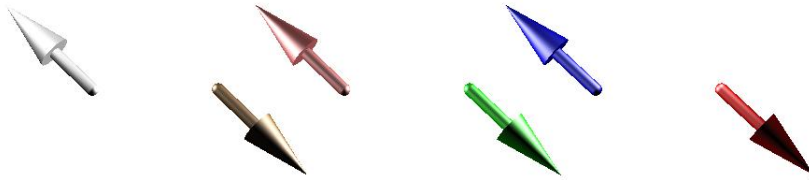
We now have the mechanism in place to model the true dynamics of lattices with nearly any type of spin-spin interaction topology: as long as the members of each sublattice depend only on the orientation of the members of a separate and independent sublattice or sublattices, this method will give the true dynamics of the system to within machine precision, both with and without dissipation. While we do expect exotic interaction topologies to exhibit unique emergent behavior, the nearest neighbor topology presented in this chapter also fulfills the requirements for a complex system described in Chapter 1 and does show emergent properties.

Complexity

An extensive analysis of the complex properties of the conservative and dissipative Heisenberg models is beyond the scope of this project, and indeed remains an open area of research. In this section, then, we will briefly discuss some of the surprising emergent properties we have observed in the development of our spin lattice model.



(a)



(b)

Figure 3.12 Equilibrium states of the dissipative spin lattice showing the effect of the sign of the coupling parameter J . (a) $J = 0.5$ for a 1D lattice of 6 spins with random initial orientations after many time steps. (b) $J = -0.5$ for a 1D lattice of 6 spins with a different random initial orientation than in (a).

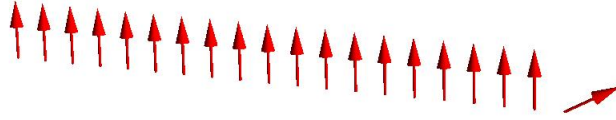


Figure 3.13 A one-dimensional lattice of 20 spins, of which 19 have zero energy (aligned) and 1 has non-zero energy (not aligned).

Based solely on the description of the interaction, we would certainly expect the non-dissipative spin lattice described in the previous section to exhibit complex behavior, and this expectation is certainly borne out by one immediately observable characteristic of such a system: energy transfer. Consider a system of 20 spins in a one-dimensional lattice, in which initially all spins are exactly aligned except one (see Fig. 3.13), which points in a different direction and thus has a given amount of energy with respect to the direction of alignment of the other spins. If we allow this system to evolve according to the Suzuki-Trotter algorithm developed in the previous section, it is apparent that the spins will not remain aligned over time. The value

$$E = 1 - \mathbf{S}_0 \cdot \mathbf{S}_i(t), \quad (3.34)$$

where \mathbf{S}_0 represents the initial orientation of the aligned spin vectors and $\mathbf{S}_i(t)$ is the orientation of spin i after time t , can be used as a crude indicator of the energy of each spin—that is, how far it has deviated from the initial alignment of the aligned spins (which is taken as zero energy). Plotting this value for the initially unaligned spin and the middle spin indicates that the deviation from the initial alignment “travels” through the lattice, so that when spin 10 (which was initially aligned) reaches a large energy value, spin 20 (which was initially given energy) now has nearly zero energy. This occurs for all spins in the lattice—some with more energy, some with less; thus, the initial energy becomes distributed throughout the lattice as expected,

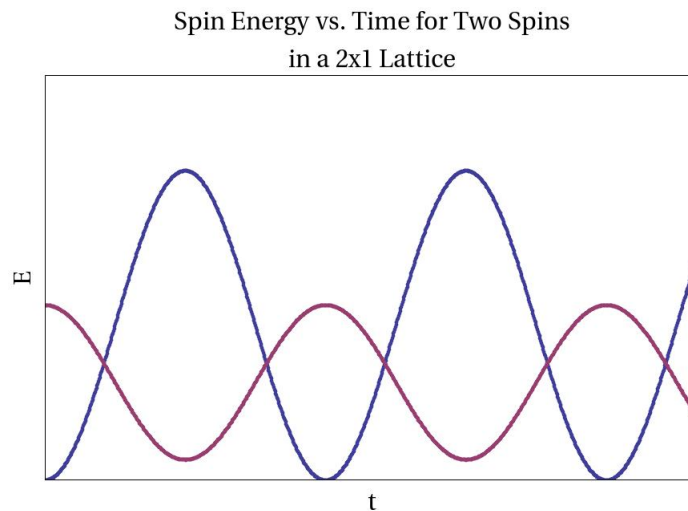


Figure 3.14 Spin energy calculated using Eq. 3.34 for a 2×1 spin lattice. In this case, the total energy is essentially shuttled back and forth between the spins. The apparent “violation” of the principle of conservation of energy is due to the simplistic algorithm used to measure the energy of each spin (Eq. 3.34).

but also exhibits a tendency to move from one spin to another *without becoming evenly distributed*, rather like a coupled spring system. In fact, a system of only two spins will tend to shift energy between the two spins exactly in the manner of two spring-coupled masses, as shown in Fig. 3.14. Fig. 3.15 shows energy (calculated using Eq. 3.34) as a function of time for the middle and last spin in a one-dimensional lattice of 20 spins (as in Fig. 3.13). If we treat a single spin in the lattice as a system in and of itself, we have a system in which energy enters and exits according to the rules of the surrounding “heatbath” (i.e. the rest of the lattice). However, from the perspective of the single spin, all it sees is essentially a “random” sequence of driving and damping. In analogy to the driven, damped pendulum, there is a significant possibility that this “driven-damped” single-spin system also exhibits chaotic behavior, a possibility that is qualitatively supported by the graph of the trajectory of a single spin in the undamped spin lattice shown in Fig. 3.16. In addition to suggesting chaotic activity in the trajectories of individual spins, from a holistic perspective this inter-spin energy

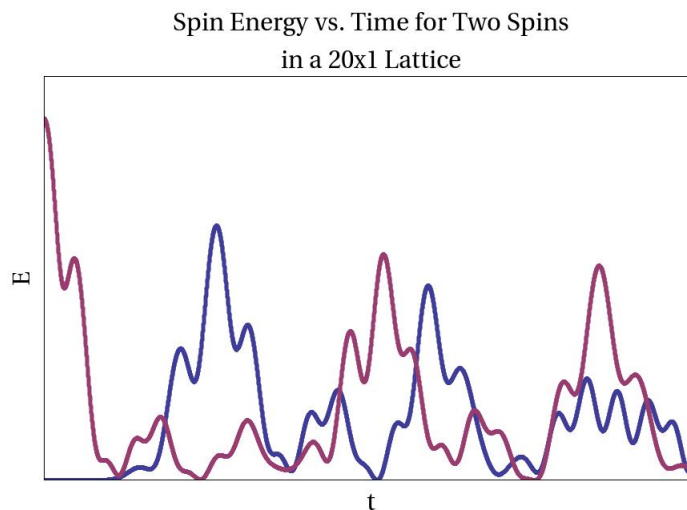


Figure 3.15 Spin energy calculated using Eq. 3.34 for two spins in a one dimensional lattice of 20 spins. The red line is for spin 20, which was given initial energy, while the blue spin is for spin 10, which was initially aligned. Note the time delay before the energy reaches the middle and note that the peak energy is generally out of phase for these two spins.

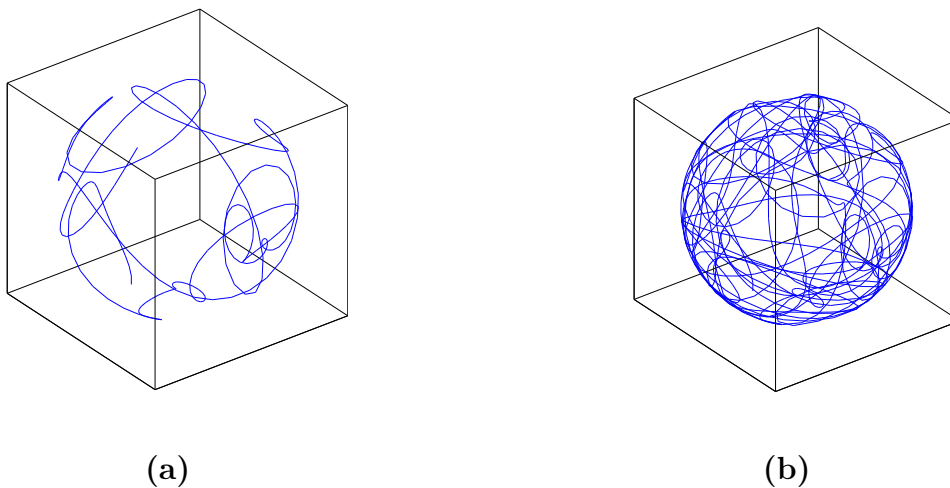


Figure 3.16 Three dimensional trajectory for a single spin in a $4 \times 4 \times 4$ spin lattice. (a) shows the trajectory after 250 time steps. (b) shows the same trajectory after 1000 steps.

transfer is also a strong indication of the presence of spin waves in the lattice. We have not made systematic efforts to find spin waves in our model, but other researchers using similar algorithms have demonstrated the presence of spin waves in comparable models [1, 2, 23].

The most exciting emergent phenomenon exhibited by our model is the spontaneous onset of magnetic domains in the dissipative case. As explained in the previous section, over long periods of time the dissipative spin lattice will eventually reach an equilibrium state in which all spins are aligned or all spins are anti-aligned. For small lattices with a random initial configuration, this convergence occurs quite quickly with few notable emergent features (for $J > 0$, spin waves appear to form near equilibrium but quickly die out as the total energy in the system goes to zero). However, in the case of large lattices with a random initial configuration, the system takes much longer to reach the equilibrium state, and it is this intermediate, dynamical state that is of much physical interest. With $J > 0$, as the system evolves patches of like spin begin to form, which continue to grow as energy leaves the system (For $J < 0$, patches of anti-aligned spins form with similar properties but much faster convergence). This is easiest to observe by using a two-dimensional lattice and assigning colors to specific directions and plotting squares of color corresponding to the directions of the spin vectors rather than the spin vectors themselves as arrows. For example, areas containing spins pointing in the \hat{z} direction could be colored red, while areas containing spins pointing in the $-\hat{z}$ direction could be colored blue. Areas with spins pointing somewhere between these two directions should be colored so as to indicate their proximity to the two extremes, as shown in Fig. 3.17. The result is the clear emergence of regions of color corresponding to regions of like spin, bounded by regions of intermediate spins, which can be qualitatively understood as emergent magnetic domains in a meta-stable state (see Fig. 3.18).

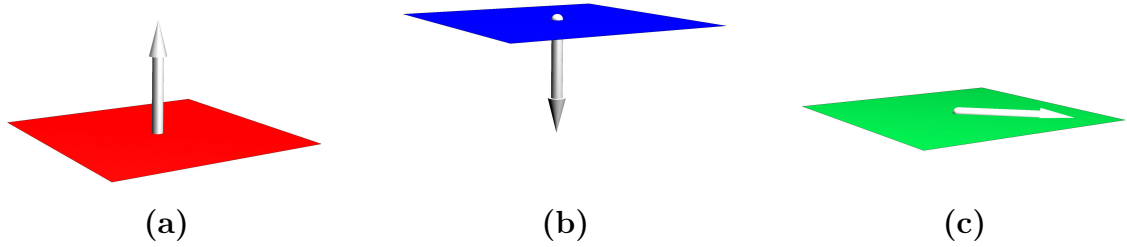


Figure 3.17 Example of mapping spin orientations to colors: (a) Spaces containing spins pointing in the $+\hat{z}$ direction may be colored red. (b) Spaces for spins pointing in the $-\hat{z}$ direction may be colored blue. (c) Spaces for spins pointing between the two extremes can be represented by an intermediate color.

The graphs in Fig. 3.18 were made by taking advantage of Matlab’s *pcolor* command, which automatically assigns a color gradient to a given numerical range. However, in order to view domain formation in three dimensions, additional care must be taken to allow the true three dimensional nature of the domains to be visualized correctly. We did this by assigning a transparency level to the unit volumes containing the intermediate spins, in addition to an intermediate color, according to the equation

$$\alpha = |z|^x,$$

where α is a fraction representing the desired opacity level (0 representing full transparency to 1 representing full opacity), z is the spin direction contained within the volume to be drawn, and x is an adjustable parameter that determines how quickly volumes containing small values of z will become opaque (higher values result in smaller, but more visible domains throughout the three dimensional lattice). Based on this idea, we developed a *pcolors3D* function that is analogous to Matlab’s native *pcolor* function, but creates a three-dimensional pseudocolor volume plot with a specified transparency falloff. The code for this function is given in Appendix D. The results obtained are very similar to those observed in the two-dimensional case, but with magnetic domains extending into three dimensions, as shown in Fig. 3.19.

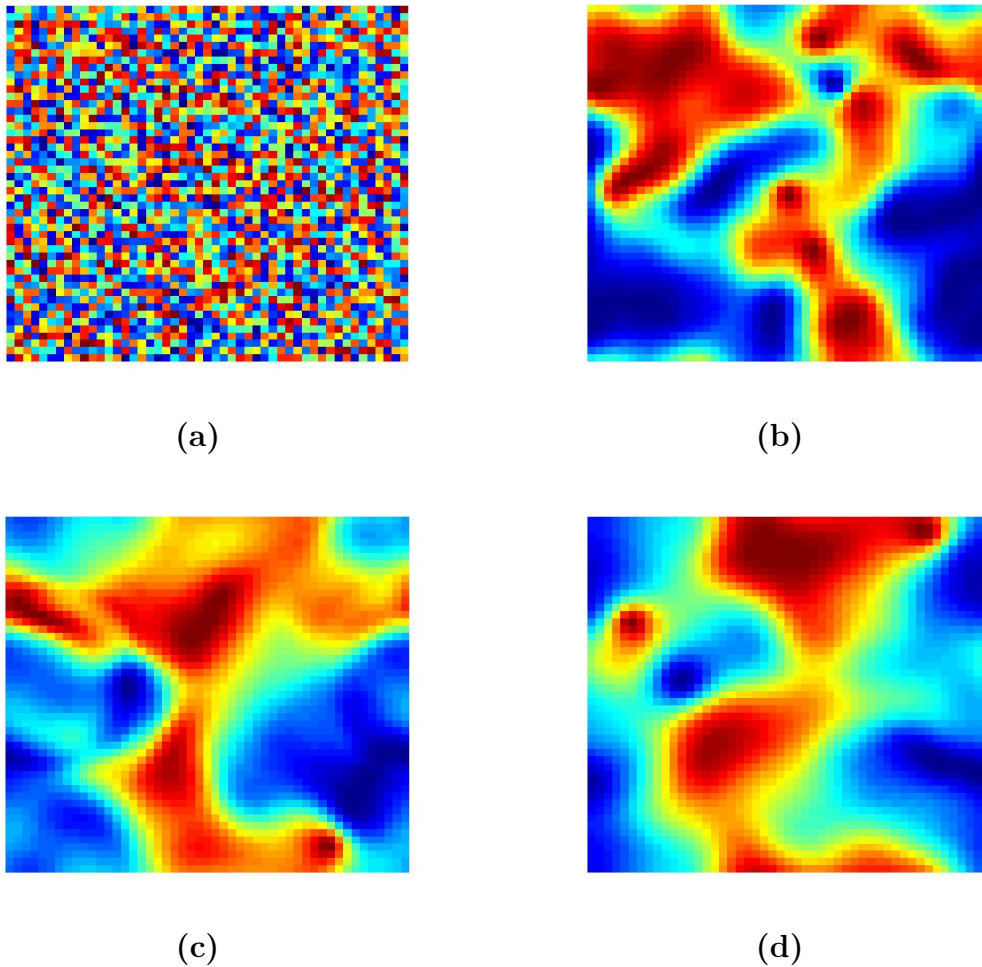


Figure 3.18 Sequence of figures showing emergence and evolution of magnetic domains in a $50 \times 50 \times 1$ damped spin lattice during 1000 time steps. Dark blue and dark red represent spin vectors pointing very near perpendicular to the plane of the page in opposite directions. Note the coalescence and growth of the red spin domains as time advances. (a) Initial random state $t = 0$. (b) After 500 time steps, domains are clearly visible. (c) $t = 750$. (d) $t = 999$.

The emergence of magnetic domains in the damped Heisenberg model is a demonstration of the complexity inherent in the system: a lattice of non-linearly coupled particles with a non-linear dissipation factor that inhibits the free exchange of energy between particles.

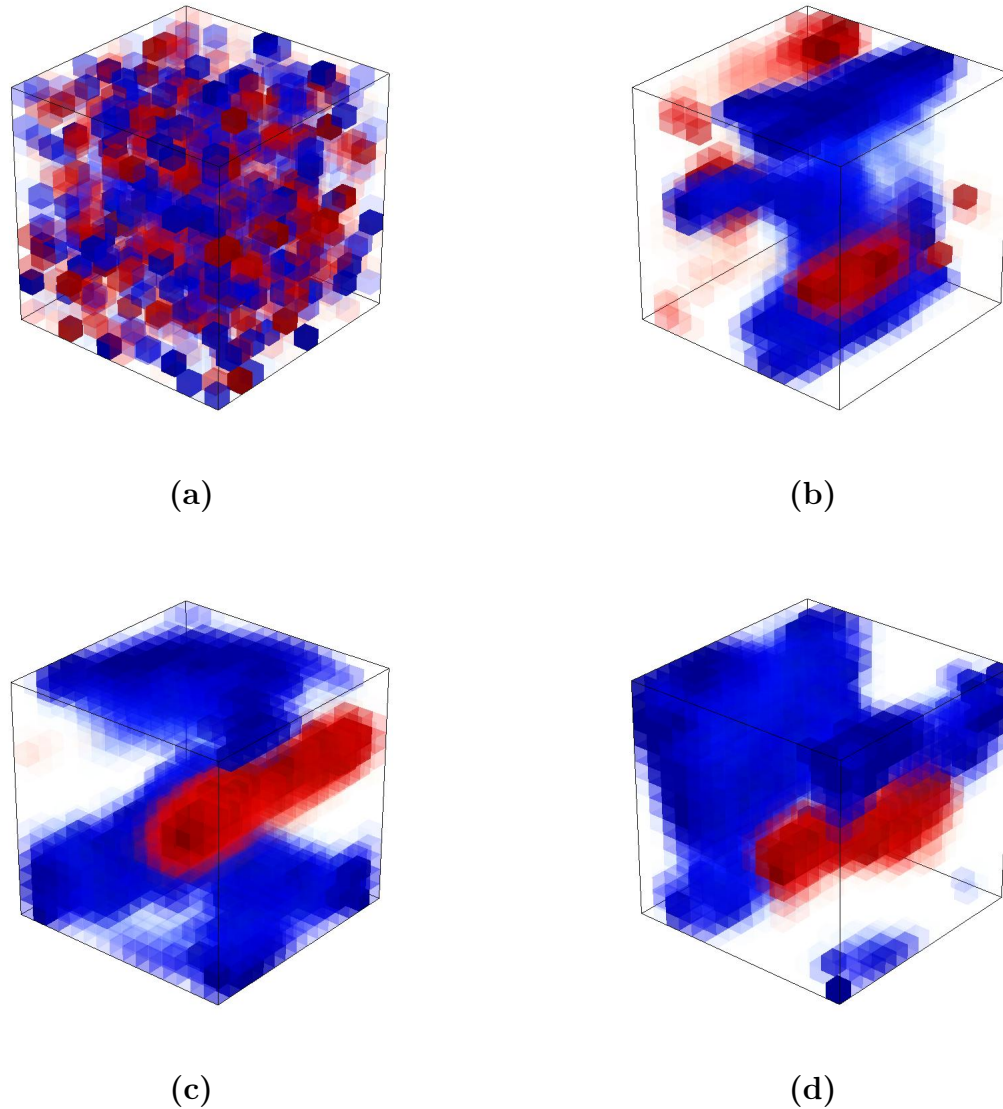


Figure 3.19 Sequence of figures showing the emergence and evolution of magnetic domains in three dimensions for a damped $15 \times 15 \times 15$ lattice for 500 time steps. Dark red and dark blue cubes represent spins pointing nearly vertically up or down (\hat{z} direction), while lighter shades represent some deviation from that orientation. The empty space corresponds to the yellow and green areas in Fig. 3.18; however, in this case the corresponding spaces were left transparent to reveal the true three-dimensional nature of the domains formed by the red and blue regions. (a) The original random configuration. (b) After 250 time steps domains are clearly evident. (c) After 380 time steps. (d) After 500 time steps.

Chapter 4

Conclusion

Emergent properties are one of the hallmarks of a complex, dynamical system, and frequently represent the macroscopic, physically observable characteristics of the system. While the emergence of these properties is clearly due to the “first principles” laws that govern the observable universe, in a complex system the link between these basic laws and the observed emergent order may be impossible to find, especially in light of the fact that this order may be dynamic in nature and may occur far from the equilibrium state of the system. Frequently, however, such emergent properties can be explained through the coupling of dimensions in a multi-dimensional representation of the system—that is, it is possible to define a set of dynamical rules (based on a physical understanding of the system) that determines how the system will evolve in a certain dimension based on the effects and influence of the others. The number and nature of the dimensions into which a system can be divided depends strongly on the physical nature of the system, as well as the rules for dimensional coupling. For example, referring to the flocking model presented in Chapter 2, each boid can be considered a representation of two dimensions (v_i, θ_i) of the entire $2N$ -dimensional flock. This is convenient because there is a clear physical interpretation for dimen-

sional coupling: each boid interacts in some way with its surrounding flockmates. In the absence of any dimensional coupling (each boid flies in a straight line regardless of the direction or proximity of any other members of the flock), the dynamics of the flock as a whole become essentially random, even though individual motions are easily understood and interpreted. In a sense, this decoupling of the phase space reduces the flocking model to a dilute gas, as discussed in Chapter 1. The inclusion of dimensional coupling, however, can give rise to emergent dynamic order in the flock, where the exact details of such order are highly dependent on the strength of the coupling (number of neighbors in the flocking case) and on the initial conditions (see Fig. 2.4).

As discussed in Chapter 1, emergent behavior will only occur if the dimensional couplings in the system inject some sort of non-linearity into the dynamics of the system. These non-linearities, in a sense, “drive” the system toward emergence rather than averaging out across multiple dimensions as would occur with linear interactions. In our boids model, the non-linearity that produces the emergent behavior is subtle, but drives the onset of the various phases of equilibrium motion shown in Fig. 2.2 and is critical to the vast range of emergent behavior that arises in the presence of frustration, as shown in Figs. 2.3 and 2.4. This non-linearity appears as a “violation” of conservation of energy (which will occur in any open system) resulting from the fact that each boid moves at a constant speed, as implied by Eq. 2.1 and shown explicitly in equation 2.3. Nevertheless, despite the non-linearity of the dimensional coupling, the consensus-only boids model is only capable of uniform motion (albeit three types), which is quantified in Appendix A.

In the Heisenberg model discussed in Chapter 3, dimensional coupling is given by the spin-spin interaction explained in the section on multiple spin dynamics beginning on page 38, and mathematically quantified in Eq. 3.27. As with the boids model,

there is a clear physical interpretation associated with the dimensional coupling—in fact, the nearest neighbors interaction is very well known in spin dynamics and the dimensional coupling is essentially a recasting of a well-understood interaction in terms of complexity theory. Unlike the boids model however, in the absence of damping, this coupling is not sufficient to give rise to complex or emergent behavior. This lack of emergent behavior suggests uniformity in the phase space of the model, which is clearly illustrated by the plot of total magnetization over time, shown in Fig. 3.11. In spite of the fact that energy is transferred from spin to spin throughout the system, the undamped Heisenberg model cannot exhibit emergence—the interactions tend to average out over time resulting in constant magnetization.

Both the consensus-only boids model and the undamped Heisenberg model are of significant physical interest, especially from the perspective of statistical mechanics. However, they gain additional importance as complex systems with the addition of an antagonistic factor that tends to amplify the non-linearity of both the boids model and the Heisenberg model. In both cases, this antagonistic factor is critical to the onset of the emergent properties shown in Figs. 2.3, 2.4, 3.18, and 3.19.

In the case of the boids model, it is the boundary that provides the antagonistic “frustration” as it was termed in Chapter 2 and prevents the boids from reaching any of the more uniform coherent states shown in Fig. 2.2. Furthermore, it seems that the reflection by π at the boundary serves to further amplify the non-linearity inherent to the system, thus providing an additional angular momentum “kick” to the entire system each time a boid reaches the boundary. The resulting dynamics are cohesive and highly resistant to the continuous perturbations to the flock imposed by the boundary—that is, although the boundary tends to break the flock’s tendency toward complete coherence, it is unable to destroy the cohesiveness of the flock and serves to alter the physical shape and dynamics of the flock as a whole.

In the Heisenberg model, as alluded to in Chapter 3, the Gilbert damping term provides a sufficiently strong non-linear antagonistic factor to allow the onset of emergent phenomena. It is the damping term that injects the required extra non-linearity into the system. As in all complex systems, it is the non-linearity that drives the system toward emergence, where in this case, we observe the emergence of meta-stable magnetic domains as energy is continually drained from the system. Whether other emergent phenomena will arise if alternate interaction topologies are used (potentially amplifying the non-linearity introduced by the damping term or injecting additional non-linear factors) remains an open question.

Emergent phenomena in complex systems depend critically on the presence of non-linear dimensional coupling within the system. As illustrated by both the non-interacting boids model and the Heisenberg model in the presence of a very strong external field, if the dimensions of the system are decoupled, the dynamics of the entire system can be easily represented by a single set of dimensions. In other words, nothing is gained by observing the dynamics of N boids in $2N$ dimensions since only 2 of those dimensions are unique and the remaining dimensions are statistically identical. Likewise, an array of N spins with random energies precessing about a very strong external magnetic field offers no information that could not be had by allowing a single spin to precess about an identical field at various energies. Only by coupling the dimensions in each system do the dynamics occurring in each dimension become unique, but related so as to induce emergent phenomena on a system-wide scale. The additional presence of an antagonistic factor that prevents the non-linearity from driving the system to a uniform equilibrium state will tend to enhance the emergent dynamics, which are generally most interesting and least tractable far from any equilibrium state.

While such emergent phenomena frequently defy analysis by traditional reduction-

ist methods, the imposition of additional layers of abstraction in terms of non-linearly coupled dimensions and antagonistic factors may allow us to create sets of rules governing the onset of many types of emergent order. Only such a holistic approach will allow us to come to a deeper understanding of the complex, macroscopic phenomena that have so frequently eluded sequestration by simple physical laws, and may possibly lead us to ever greater insights into the fundamental laws that govern the Universe.

Bibliography

- [1] V. P. Antropov, M. I. Katsnelson, B. N. Harmon, M. van Schilfgaarde, and D. Kusnezov. Spin dynamics in magnets: Equation of motion and finite temperature effect. *Physical Review B*, 54(2):1019–1035, 1996.
- [2] T. Arponen and B. Leimkuhler. An efficient geometric integrator for thermostatted anti-/ferromagnetic models. *BIT Numerical Mathematics*, 44:403–424, 2004.
- [3] P. Bak. *How Nature Works*. Copernicus Springer-Verlag, 1996.
- [4] M. Ballerini, N. Cabibbo, R. Candelier, A. Cavagna, E. Cisbani, I. Glardina, V. Lecomte, A. Orlandi, G. Parisi, A. Procaccini, M. Viale, and V. Zdravkovic. Interaction ruling animal collective behavior depends on topological rather than metric distance: Evidence from a field study. *Proceedings of the National Academy of Sciences*, 105(4):1232–1237, January 2008.
- [5] Ch. Becco, N. Vandewalle, J. Delcourt, and P. Poncin. Experimental evidences of a structural and dynamical transition in fish school. *Physica A*, 367:487–493, 2006.
- [6] J. M. Davis. The coordinated aerobatics of dunlin flocks. *Animal Behavior*, 28:668–673, 1980.

-
- [7] V. Dossetti, F. J. Sevilla, and V. M. Kenkre. Phase transitions induced by complex nonlinear noise in a system of self-propelled agents. *Physical Review E*, 79(5):051115–1–051115–11, 2009.
- [8] L. Fisher. *The Perfect Swarm*. Basic Books, 2009.
- [9] J. Gleick. *Chaos: Making A New Science*. Penguin Books, 1988.
- [10] B. Goodwin and R. Solé. *Signs of Life: How Complexity Pervades Biology*. Basic Books, New York, 2000.
- [11] G. Grégoire and H. Chaté. Onset of collective and cohesive motion. *Physical Review Letters*, 92(2):025702–1–025702–4, January 2004.
- [12] R. D. Gregory. *Classical Mechanics*. Cambridge University Press, 2006.
- [13] F. Heppner and U. Grenander. A stochastic nonlinear model for coordinated bird flocks. In S. Krasner, editor, *The Ubiquity of Chaos*, pages 233–238. American Association for the Advancement of Science, Washington, DC, 1990.
- [14] K. Huang. *Lectures on Statistical Physics and Protein Folding*. World Scientific Publishing Company, Inc., River Edge, NJ, 2005.
- [15] M. Lakshmanan and K. Nakamura. Landau-Lifshitz equation of ferromagnetism: Exact treatment of the Gilbert damping. *Physical Review Letters*, 53(26):2947–2499, December 1984.
- [16] E. Magyari, H. Thomas, and R. Weber. Comment on Landau-Lifshitz equation of ferromagnetism: Exact treatment of the Gilbert damping. *Physical Review Letters*, 56(16):1756, April 1986.

-
- [17] R. M. May. Simple mathematical models with very complicated dynamics. *Nature*, 261:459, June 1976.
- [18] M. Mitchell. *Complexity: A Guided Tour*. Oxford University Press, New York, New York, 2009.
- [19] W. K. Potts. The chorus-line hypothesis of manoeuvre coordination in avian flocks. *Nature*, 309:344–345, May 1984.
- [20] C. W. Reynolds. Flocks, herds, and schools: A distributed behavioral model. *Computer Graphics*, 21(4):25–34, 1987.
- [21] H. E. Stanley. *Introduction to Phase Transitions and Critical Phenomena*. Oxford University Press, Oxford, 1971.
- [22] J. Toner and Y. Tu. Flocks, herds, and schools: A quantitative theory of flocking. *Physical Review E*, 58(4):4828–4858, October 1998.
- [23] S.-H. Tsai, H. K. Lee, and D. P. Landau. Molecular and spin dynamics simulations using modern integration methods. *American Journal of Physics*, 73(7):615–624, 2005.
- [24] T. Vicsek, A. Czirók, E. Ben-Jacob, I. Cohen, and O. Shochet. Novel type of phase transition in a system of self-driven particles. *Physical Review Letters*, 75(6):1226–1229, August 1995.

Appendix A

Phase Transitions in a Dynamic Flocking Model

One convenient method for quantifying the various types of coherent motion observed in our topological flocking model with periodic boundary conditions (Chapter 2) can be found in the concept of phase transitions and order parameters [5, 7, 11, 22, 24]. Fig. 2.2 shows the various types or phases of coherent motion exhibited by the model. As described in the chapter, these phases arise entirely due to the initial random configuration of boids and represent a dynamic equilibrium state of the system from that particular configuration. However, by introducing a small random element based on a control parameter η into the equations of motion, it is possible to destabilize the equilibrium so as to induce transitions from one phase of motion to another by adjusting η , analogous to inducing a change of state in a material by adjusting the temperature.

A practical way to do this is by adding a random angle $\Delta\theta$ to the average velocity $\bar{\mathbf{v}}$ calculated in Eq. 2.3. Thus

$$\bar{\mathbf{v}}' = \bar{\mathbf{v}} + \cos(\Delta\theta)\hat{i} + \sin(\Delta\theta)\hat{j},$$

where $\Delta\theta$ is a random number calculated with uniform probability on the interval $[-\eta/2, \eta/2]$, $\bar{\mathbf{v}}$ is calculated according to equation 2.3 and $\bar{\mathbf{v}}'$ is appropriately normalized in keeping with the constant speed required by the model. Our simulations have shown that this random element is in fact analogous to temperature-induced noise in a system of free particles and allows the system of boids to transition from one phase of motion to another.

In order to determine computationally whether a phase transition has occurred, it is necessary to establish a mathematical description of each phase of motion, known as an order parameter [14, 21]. In general, an adequate order parameter will have a range in the interval $[0, 1]$, where 1 represents complete order within the system, and 0 indicates that the order described by the order parameter is not present in the system. It should be noted that a value of zero does not necessarily indicate disorder in the system—it only indicates the absence of the ordered state described by the order parameter. A different order parameter could demonstrate the presence of a completely different ordered state—a fact we will take advantage of in our analysis of our flocking model.

The aligned phase of our flocking model (Fig. 2.2) can be physically described as coherent linear motion among all members of the flock. Mathematically, an appropriate order parameter to describe this phase of motion is given by the absolute value of the average, normalized velocity of all the boids [24], which can be calculated by

$$\langle v \rangle = \frac{1}{Nv_0} \left| \sum_{i=1}^N \mathbf{v}_i \right|, \quad (\text{A.1})$$

where N is the total number of boids and v_0 is the speed of the boids (constant in our model). As expected, this value is very close to zero for completely random motion, and it is also zero for both of the circular phases shown in Fig. 2.2, as it is based on the vector sum of the boid velocities. Accordingly, it approaches one in the completely

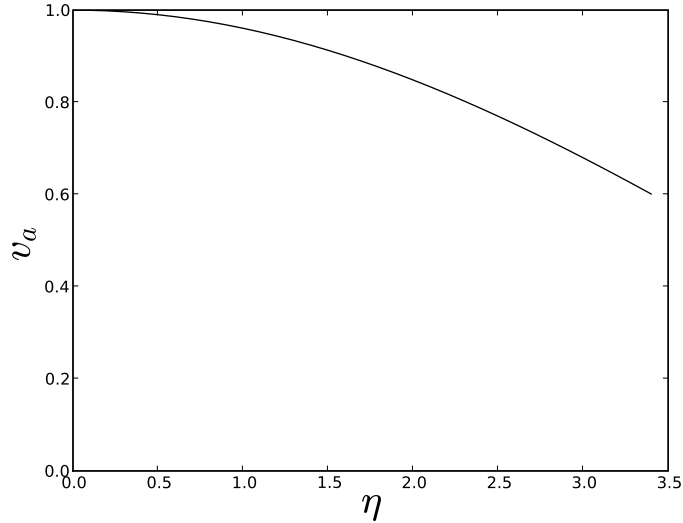


Figure A.1 Graph showing a phase transition from aligned, linear motion to essentially random motion as noise parameter η is increased

aligned phase (that is, when $\eta = 0$) is reached. By plotting $\langle v \rangle$ against increasing noise η for a fixed number of boids, we can observe the transition from fully aligned motion to nearly random motion, as shown in Fig. A.1.

While Eq. A.1 does account for aligned motion, it does not differentiate between the random phase and the two circular phases of motion, as the vector sum over all boids tends to vanish for each of these phases (as is clear by inspection of a snapshot of these phases of motion, see Fig. 2.2). Therefore, using this order parameter alone renders the circular phases indistinguishable from the random phase.

The rotational phases can be quantified using a new order parameter inspired by the concept of angular momentum. We can thus define a rotational order parameter \mathcal{L} by using the antisymmetrized product of the velocity vectors (the wedge product \wedge) taken at two consecutive time steps and averaging both over time and over the entire flock:

$$\mathcal{L} = \frac{1}{N} \sum_{i=1}^N \frac{1}{z} \sum_{n=1}^z \frac{\mathbf{v}_i(n) \wedge \mathbf{v}_i(n+1)}{v_0^2}, \quad (\text{A.2})$$

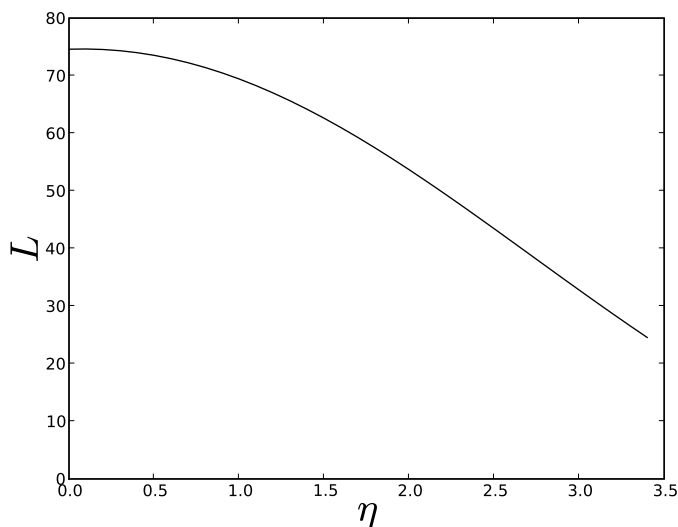


Figure A.2 Graph illustrating a phase transition from rotational motion to random motion as noise parameter η is increased.

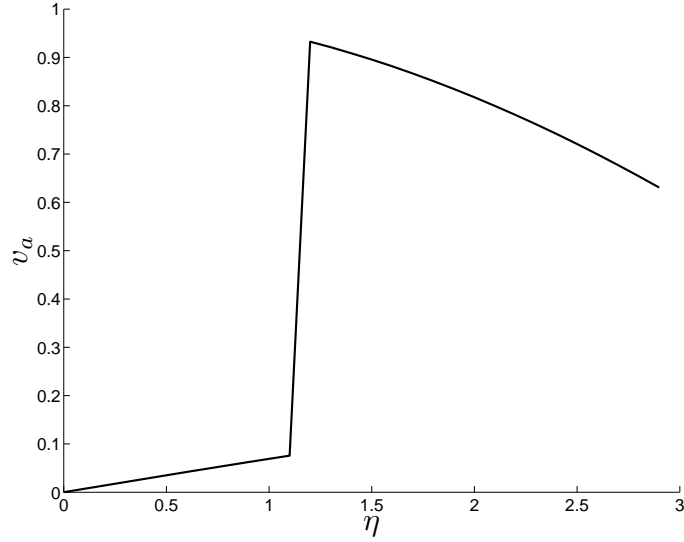
where z represents a sufficiently large number of iterations to ensure an accurate time average and thus make an accurate determination of the true dynamic coherence.

As in the case of $\langle v \rangle$, Eq. A.2 will go to zero in the case of random motion. It also goes to zero for aligned motion. However, if the system enters a rotational phase, \mathcal{L} will approach a positive or negative non-zero value depending on the direction of rotation. Because \mathcal{L} depends on the time required to execute a loop (or at least a distinguishable portion thereof), it will most likely not approach unity as η goes to zero; however, it will reach sufficiently large positive or negative values (often with an absolute value much greater than 1) to distinguish between both rotational phases and to distinguish the rotational phases from linear and random motion. Fig. A.2 shows a plot of Eq. A.2 against η , illustrating the phase transition from counter-clockwise rotational motion to random motion.

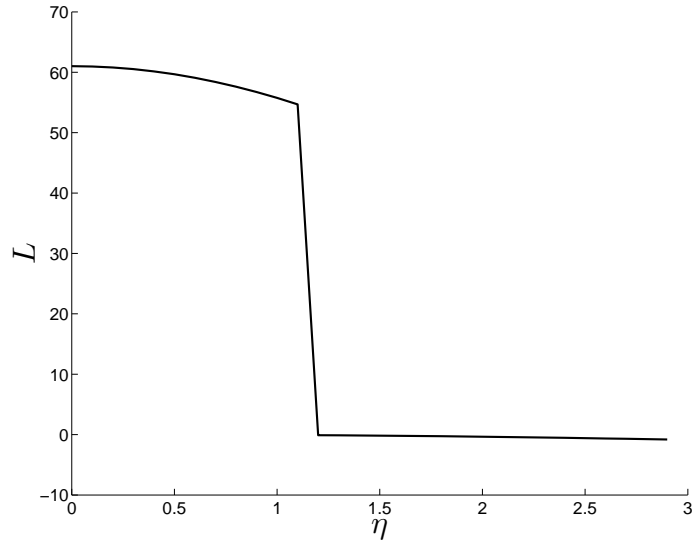
Using Eqs. A.1 and A.2, we have demonstrated that our non-bounded flocking model exhibits phase transitions between the various types of ordered motion shown

in Fig. 2.2 and random motion (also shown in Fig. 2.2). However, and possibly of more physical interest, is the fact that this model also exhibits phase transitions between the aligned and rotational phases. That is, the model will frequently undergo a spontaneous shift from the aligned phase to a rotational phase and *vice versa* with only a small change in η . This is typically difficult to see in the animations directly, as it frequently occurs for larger values of η ($\eta > 2.5$), and the phase shift is drowned out visually by noise-induced random motion. However, the phase transition is very clear in plots of the order parameters $\langle v \rangle$ and \mathcal{L} . Fig. A.3 shows plots of $\langle v \rangle$ and \mathcal{L} for a phase transition directly from aligned motion to rotational motion.

Our topological flocking model exhibits richer motion than typical nearest-neighbor models. By defining the appropriate order parameters, we can demonstrate the existence of dynamic phase transitions in our model, thus providing a method of direct, quantifiable comparison between our model and other models. Furthermore, we also lay the groundwork for a statistical mechanical analysis of the much richer motion exhibited by the addition of frustration as explained in the main body of this text.



(a)



(b)

Figure A.3 Graphs showing a phase transition directly from rotational motion to linear motion as noise parameter η is increased. (a) Plot of average velocity $\langle v \rangle$ showing phase change near $\eta = 1.15$. (b) Plot of Eq. A.2 for the same configuration as in (a) showing the onset of rotational motion near $\eta = 1.15$.

Appendix B

An Analytic Solution to the Gilbert Damping Equation

Even though Eq. 3.6 is non-linear, it can in fact be solved analytically, for a constant local field \mathbf{H} and a fixed reference frame, as a set of coupled differential equations in Cartesian space. Taking the full vector construction of the Gilbert relaxation equation (Eq. 3.6) and using Eq. 3.2 to expand the cross product in the first term, we have

$$\frac{\partial}{\partial t} \begin{pmatrix} S_x \\ S_y \\ S_z \end{pmatrix} = - \begin{pmatrix} 0 & -H_z & H_y \\ H_z & 0 & -H_x \\ -H_y & H_x & 0 \end{pmatrix} \begin{pmatrix} S_x \\ S_y \\ S_z \end{pmatrix} + \lambda(\mathbf{S} \cdot \mathbf{S})\mathbf{H} - \lambda(\mathbf{S} \cdot \mathbf{H}) \begin{pmatrix} S_x \\ S_y \\ S_z \end{pmatrix}. \quad (\text{B.1})$$

This equation can be separated into its x , y , and z components, forming three coupled differential equations

$$\frac{\partial S_x(t)}{\partial t} = H_z S_y(t) - H_y S_z(t) - \lambda(\mathbf{H} \cdot \mathbf{S}(t)) S_x(t) + \lambda(\mathbf{S}(t) \cdot \mathbf{S}(t)) H_x, \quad (\text{B.2a})$$

$$\frac{\partial S_y(t)}{\partial t} = -H_z S_x(t) + H_x S_z(t) - \lambda (\mathbf{H} \cdot \mathbf{S}(t)) S_y(t) + \lambda (\mathbf{S}(t) \cdot \mathbf{S}(t)) H_y, \quad (\text{B.2b})$$

$$\frac{\partial S_z(t)}{\partial t} = H_y S_x(t) - H_x S_y(t) - \lambda (\mathbf{H} \cdot \mathbf{S}(t)) S_z(t) + \lambda (\mathbf{S}(t) \cdot \mathbf{S}(t)) H_z. \quad (\text{B.2c})$$

If we consider a constant magnetic field and take the \hat{z} direction to be the direction of that field, the foregoing equations reduce to

$$\frac{\partial S_x(t)}{\partial t} = H_z S_y(t) - \lambda H_z S_x(t) S_z(t), \quad (\text{B.3a})$$

$$\frac{\partial S_y(t)}{\partial t} = -H_z S_x(t) - \lambda H_z S_y(t) S_z(t), \quad (\text{B.3b})$$

$$\frac{\partial S_z(t)}{\partial t} = -\lambda H_z S_z(t)^2 + \lambda H_z (\mathbf{S} \cdot \mathbf{S}). \quad (\text{B.3c})$$

Since Eq. B.3c depends only on the z component of \mathbf{S} , and since $\mathbf{S} \cdot \mathbf{S} = S^2$ is assumed to be constant, based on the physical understanding of the model (see proofs in Chapter 3), Eq. B.3c can be solved independently of the other two and this solution can be substituted in for S_z in Eqs. B.3a and B.3b. These two equations can then be solved by defining a complex variable $\eta = S_x + i S_y$, which reduces the set of coupled differential equations to a single equation in η , which can be solved by the traditional methods. A similar approach was used by Lakshmanan and Nakamura [15], who obtained the following solution

$$S_x = \frac{2 (S_{x0} \cos(Ht) + S_{y0} \sin(Ht)) e^{-\lambda Ht}}{(1 + S_{z0})^2 + (S_{x0}^2 + S_{y0}^2) e^{-2\lambda Bt}}, \quad (\text{B.4a})$$

$$S_y = \frac{2 (S_{y0} \cos(Ht) - S_{x0} \sin(Ht)) e^{-\lambda Ht}}{(1 + S_{z0})^2 + (S_{x0}^2 + S_{y0}^2) e^{-2\lambda Bt}}, \quad (\text{B.4b})$$

$$S_z = \frac{(1 + S_{z0})^2 - (S_{x0}^2 + S_{y0}^2) e^{-2\lambda Ht}}{(1 + S_{z0})^2 + (S_{x0}^2 + S_{y0}^2) e^{-2\lambda Ht}}. \quad (\text{B.4c})$$

This solution is easily shown to be a true analytic solution to Eqs. B.2a, B.2b, and B.2c in Cartesian space.

Appendix C

Alternate Derivation of the Stereographic Projection

We begin by defining the inverse of a vector under the assumption that such an inverse can be defined and that a multiplication allowing such an inverse can also be defined. Geometrically, we can understand the inverse of a vector by analogy from the one-dimensional case on the number line. Fig. C.1 shows a geometric diagram of the inverse of such a scalar value. Note that the inverse of 1 is 1, and the inverse of a scalar simply represents a one-dimensional reflection about 1. We now consider many such number lines pointing radially outward from the origin, thus any given distance from the origin forms a sphere centered at the origin. The inverse of a vector can now be geometrically represented as a reflection across the unit sphere analogous to the

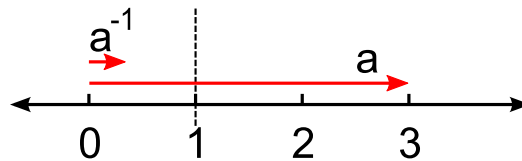


Figure C.1 Inverse of a scalar shown geometrically. Notice that the inverse maps the range $1 < a < \infty$ to the range $0 < a^{-1} < 1$ and *vice versa* by reflection about 1.

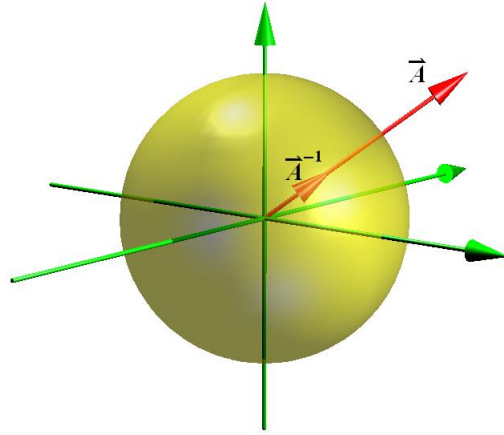


Figure C.2 Inverse of a vector shown geometrically by analogy to the one dimensional case. Consider a number line along the direction of vector \mathbf{A} . Then \mathbf{A}^{-1} is simply a reflection across the unit sphere, shown here in yellow. The green arrows represent the regular Cartesian coordinate system. Compare with Fig. C.1.

one dimensional case, as shown in Fig. C.2. Again, in analogy to the one-dimensional case, we take the inverse of a unit vector $\hat{\mathbf{n}}$ to be $\hat{\mathbf{n}}$, so we have

$$\mathbf{A}^{-1} = (A\hat{\mathbf{n}})^{-1},$$

but A is just a scalar while, by definition, $\hat{\mathbf{n}}^{-1} = \hat{\mathbf{n}}$, thus

$$\mathbf{A}^{-1} = \frac{1}{A}\hat{\mathbf{n}} = \frac{\mathbf{A}}{A^2}. \quad (\text{C.1})$$

To develop our conformal transformation from Cartesian to stereographic coordinates, consider a series of geometric transformations, including the vector inverse defined above: Taking a vector \mathbf{r} sharing the same origin with a normal vector $\hat{\mathbf{n}}$ describing the stereographic projection plane, we then translate these vectors by $\hat{\mathbf{n}}$. Thus

$$\mathbf{r}' = \mathbf{r} + \hat{\mathbf{n}}.$$

We now project the resulting vector \mathbf{r}' onto a different sphere using the vector inverse.

So

$$\mathbf{r}'' = \frac{1}{\mathbf{r}'} = \frac{1}{\mathbf{r} + \hat{\mathbf{n}}}.$$

Translation by $\hat{\mathbf{n}}/2$ and multiplication by 2 complete the transformation, so that ω , the transformation of \mathbf{r} , is given by

$$\omega = 2 \left(\frac{1}{\mathbf{r} + \hat{\mathbf{n}}} - \frac{\hat{\mathbf{n}}}{2} \right) = \frac{2(\mathbf{r} + \hat{\mathbf{n}})}{(\mathbf{r} + \hat{\mathbf{n}})^2} - \hat{\mathbf{n}}, \quad (\text{C.2})$$

which is identical to the Möbius transformation given in Chapter 3, and the rest of the derivation proceeds as from Eq. 3.12.

Appendix D

Code for *pcolors3D*

The following code listing is the Matlab code used for the `pcolors3D` function we developed to visualize magnetic domains in large three dimensional lattices.

```
function pcolors3D(X, Y, Z, z, transparency)
    cla

    % set up vertices for the color cubes
    vert = [0 0 0; 0 0 1; 0 1 0; ...
            0 1 1; 1 0 0; 1 0 1; ...
            1 1 0; 1 1 1];

    % set up matrices to allow each cube
    % to be easily shifted to its place
    % in the lattice
    shiftx = [1 0 0; 1 0 0; 1 0 0; ...
              1 0 0; 1 0 0; 1 0 0; ...
              1 0 0; 1 0 0];
```

```
shifty = [0 1 0; 0 1 0; 0 1 0; ...
          0 1 0; 0 1 0; 0 1 0; ...
          0 1 0; 0 1 0];
shiftz = [0 0 1; 0 0 1; 0 0 1; ...
          0 0 1; 0 0 1; 0 0 1; ...
          0 0 1; 0 0 1];

% This matrix tells patch how to connect
% the vertices
face = [1 5 7 3; 1 5 6 2; ...
        1 3 4 2; 3 4 8 7; ...
        2 4 8 6; 5 7 8 6];

% Don't draw cubes that will be transparent
% Use a number greater than zero to skip
% cubes that will be transparent anyway, for speed.
% Using zero will cause the code to draw all
% cubes, even if they are transparent.
pmask = abs(z)>0;
pindex = get_index(pmask);

% Set up lighting for cubes
lighting gouraud;
material shiny;

% Loop through cubes to be drawn and draw
```

```
% with color and transparency specified by
% z coordinate
for i=pindex
    patch('Vertices', ...
          vert+X(i)*shiftx+Y(i)*shifty+Z(i)*shiftz, ...
          'Faces', face, 'FaceVertexCData', ...
          z(i), 'FaceColor', 'flat', ...
          'EdgeColor', 'none', 'FaceAlpha', ...
          abs(z(i))^transparency);
    caxis([-1, 1])
end

% Make the plot look nice on screen
set(gca, 'Projection', 'perspective');
view([40, 28]);
axis equal tight off vis3d;
set(gcf, 'Color', 'w');
end

% This function returns a vector containing the positions of
% non-zero values of the vector representation of a given
% multidimensional matrix, m
function index = get_index(m)
    s = numel(m);
    sz = reshape(m, 1, s);
    sz = sum(sz);
```

```
ind = zeros(1,sz);
next = 1;
for i=1:s
    if m(i)>0
        ind(next) = i;
        next = next+1;
    end
end
index = ind;
end
```